

Physical Biology



PAPER

RECEIVED
10 November 2017

REVISED
25 January 2018

ACCEPTED FOR PUBLICATION
23 February 2018

PUBLISHED
30 April 2018

Coupling mechanical tension and GTPase signaling to generate cell and tissue dynamics

Cole Zmurchok¹ , Dhananjay Bhaskar² , and Leah Edelstein-Keshet¹

¹ Department of Mathematics, University of British Columbia, Vancouver, BC, Canada

² Center for Biomedical Engineering, Brown University, Providence, RI, United States of America

E-mail: zmurchok@math.ubc.ca, dhananjay_bhaskar@brown.edu and keshet@math.ubc.ca

Keywords: Rho GTPases, tension, mechanochemical coupling, collective cell behavior

Supplementary material for this article is available [online](#)

Abstract

Regulators of the actin cytoskeleton such Rho GTPases can modulate forces developed in cells by promoting actomyosin contraction. At the same time, through mechanosensing, tension is known to affect the activity of Rho GTPases. What happens when these effects act in concert? Using a minimal model (1 GTPase coupled to a Kelvin–Voigt element), we show that two-way feedback between signaling ('RhoA') and mechanical tension (stretching) leads to a spectrum of cell behaviors, including contracted or relaxed cells, and cells that oscillate between these extremes. When such 'model cells' are connected to one another in a row or in a 2D sheet ('epithelium'), we observe waves of contraction/relaxation and GTPase activity sweeping through the tissue. The minimal model lends itself to full bifurcation analysis, and suggests a mechanism that explains behavior observed in the context of development and collective cell behavior.

1. Introduction

The Rho GTPases are central regulators within signaling networks of eukaryotic cells. While their effects extend to nearly all cell functions, a primary well established role is to control the actin cytoskeleton, actomyosin assembly and myosin contraction [1]. This fact makes Rho GTPases important in regulating cell shape in single cells and in epithelia. Rac1 promotes cell spreading by activating WASP and Arp2/3, leading to dendritic actin nucleation and lamellipodial protrusion; RhoA activates ROCK, that in turn activates myosin light chain phosphorylation, and myosin-induced cell contraction. Hence, while Rac1 promotes cell spreading, RhoA counteracts this by stimulating cell contraction. While previous studies have addressed how GTPases spontaneously segregate to front or back in a cell [2–5], and how this leads to cell polarization and motility [6, 7], here we focus primarily on the effect of GTPase activity on cell contraction or spreading, and on their interplay with tension and mechanical forces experienced by cells.

Rho GTPases cycle between active and inactive forms: they are activated by guanine nucleotide-exchange factors (GEFs), and inactivated by GTPase-activating proteins (GAPs) [1]. GTPases are highly

interconnected, with crosstalk via a host of proteins. Rac1, RhoA and Cdc42 are central regulators, downstream of cell-surface receptors that sense a host of stimuli, including small ligand gradients [8], adhesion molecules, extracellular matrix (ECM), substrate stiffness [9], as well as forces and mechanical tension [10].

It has been known for many years that mechanical tension can stimulate cells and lead to signal transduction, but details of the connections were poorly understood. More recently, techniques for measuring forces felt by cells [11, 12] have been used in coordination with methods for observing activity of GTPases [13]. Such experimental work has revealed a direct connection between mechanical tension and GTPase activity in cells. Weiner and coworkers [14] showed that aspiration of neutrophil membrane by a micro-pipette directly inhibits Rac1 activity. When tension is released, Rac1 activity resumes in the cell. Experiments with atomic-force microscopy pulling on cell membrane lead to similar conclusions. Compressing cells was shown to activate RhoA [15] in a rapid and reversible way. Isotropic stretching of vascular smooth muscle cells on elastic substrate was shown to inhibit Rac1 (timescale of 5 min, recovery over 45 min) in [16]. The authors quantified GTPase activity versus % stretch, showing a decrease by about 50% in response

to a 15% stretch (figure 2(B) in [16]). How cells sense mechanical forces is reviewed in [10, 12], and the identity of multiple Rho GEFs and two GAPs involved in mechanotransduction is summarized in [17].

Cells have diverse mechanosensory mechanisms. Molecular details of the link between mechanical tension and GTPase activities are still emerging. Examples include Rap1 as a tension-sensor and its effect on Rac [18]. Tension-sensitive calcium ion channels produce signals to the Rho GTPases [15]. Integrins, vinculin, and talin act as mechanosensors that funnel signals to central regulators [19, 20]. Membrane tension is known to affect actin assembly, directly and through a PLD2-mTORC2 pathway that inhibits actin nucleation through WAVE2 [21]. Cell-substrate and cell-cell adhesion, cytoskeleton, and their effects on RhoA proteins is reviewed in [17]. Proteins such as merlin can act as a mechanochemical transducer by localizing to cortical cell-cell junctions when pulling forces are transmitted from cell to cell in epithelial tissue [22]. Focal adhesion kinase (FAK), for example, inhibits RhoA (via p190RhoGAP) and activates it (via Rgnef) in response to tension-dependent integrin reorganization, facilitating cyclic activation of RhoA and Rac1 [23]. Membrane-curvature sensing proteins such as FBP-17 and BAR domain can regulate the cycles of cell protrusion and retraction by controlling Rac1 through SLIT-ROBO GAPs (srGAPs) [24].

The connection between mechanical forces and intracellular signaling is a two-way street. On one hand, mechanical tension can influence GTPase activity. On the other hand, GTPases lead to cell deformation (spreading or contraction) that exerts pulling, stretching, or contractile forces on the cell, the local ECM, and/or neighboring cells. Hence the coupling between chemical and mechanical systems merits investigation. This observation motivates our current paper. While mechanochemical interactions have been considered in previous work [25–29], to our knowledge, this is the first instance that they are applied to a GTPase-cell and tissue dynamical system.

Rho GTPase are embedded in complex signaling networks, with many effectors, interconnections, and inputs. The details of such networks vary from one cell type to another, and adapt to cell state and environment. Nevertheless, recent experimental and modeling studies have provided evidence for the hypothesis that certain cell behaviors can be explained as emergent properties of relatively small subsets of these networks, consisting of GTPase modules. Examples of this type include the bistability and hysteresis of cell shape [30–32] and cell motility behavior [33], as well as diverse motility phenotypes in melanoma cells on patterned adhesion surfaces [28, 29]. This idea of understanding aspects of cell behavior from the dynamics of simple underlying GTPase circuits guides our approach here. Rather than attempting to describe the intricacies of signaling networks and the cytoskeleton, we focus attention on the simplest minimal GTPase

model, coupled to a minimal model for cell tension, and explore the range of emergent behavior.

Our first step is to consider a single GTPase, such as RhoA, associated with actomyosin contraction. We assume a minimal model for RhoA activity, capable of bistable dynamics and link it to feedback from mechanical tension. High RhoA activity leads the cell to contract, which results in the reduction of tension. This simple idea is explored first in a single spatially uniform cell. We characterize high or low GTPase activities and transitions between these, and the coupled dynamics of cell tension. The simplicity of this (two ordinary-differential equation) model makes it possible to fully characterize parameter-dependence and delineate regimes of behavior. Briefly, we find regimes of (1) high and (2) low RhoA (corresponding to contracted or relaxed cells) separated by (3) regimes of spontaneous, persistent cycling between these states (corresponding to cycles of contraction and relaxation in the cell).

We then consider how the minimal model plays out when many cells are mechanically coupled (e.g. by adhesion or tight junctions) in a row (1D) or in an epithelial sheet (2D). Despite the elementary aspects of the model, multicellular systems exhibit a variety of interesting behaviors. We show that, aside from overall contraction or sporadic cycling, there are waves and spatially correlated dynamical patterns of fluctuations in cell size. We simulate the model in 1D and 2D, and point to possible connections with experimentally observed cell behaviors.

In our final step, we also consider a related GTPase circuit consisting of Rac1 and RhoA (henceforth Rac and Rho). Mutual inhibition between these has been found in a number of cell types [34, 35] and highlighted in recent biological literature for both normal and malignant cells [28, 31, 33, 36, 37]. The effect of such GTPase interactions on cell shape has been explored theoretically [29, 38], but the coupling between cell shape and mechanical forces is the main theme that motivates our work here.

2. Minimal model for a single mechanochemical cell

We first considered the simplest case, where the mechanosensitivity of a single cell affects its GTPase activity (figure 1(A)), which, in turn, affects a contractile actomyosin meshwork in the cell. Our minimal model tracks the activity of a GTPase such as RhoA over time in a single cell. (While RhoA is known to redistribute intracellularly, we ignore spatial variations within a cell, so as to build a first working multicellular model.) RhoA acts through Rho-associated protein kinase (ROCK) to phosphorylate myosin light chain, leading to actomyosin contraction. Consequently, to capture the mechanical contraction, we associate a mechanical Kelvin–Voigt element (spring-dashpot system) with the cell size. In one dimension, cell size is represented by

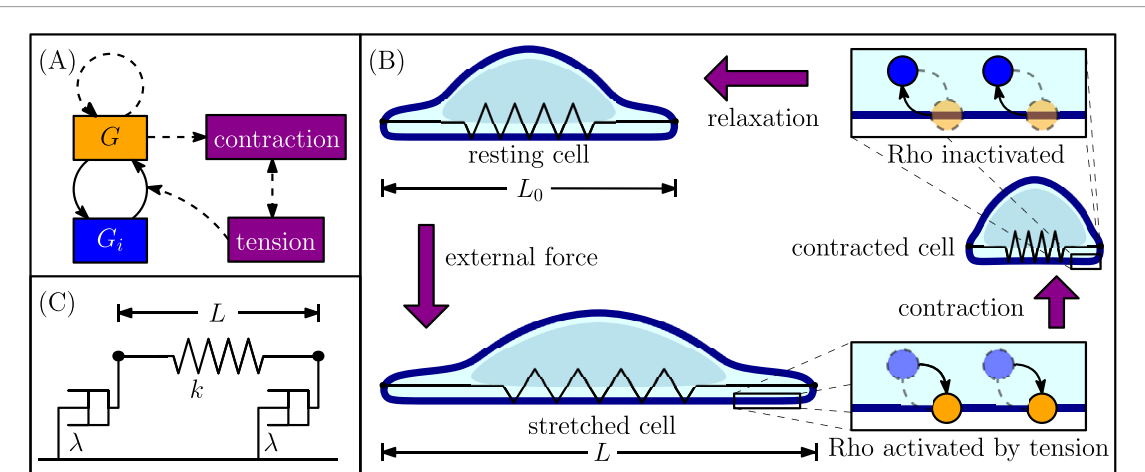


Figure 1. The minimal model for coupled GTPase activity and cellular-tension. (A) Schematic of our minimal model for a GTPase ‘mechanochemical cell’. Typical GTPase cycling between active (G , orange) and inactive (G_i , blue) forms. Black arrows denote interconversion (solid), and positive feedback (dashed) from the active GTPase and from tension to GTPase activation. Purple elements (in (A) and (B)) represent mechanical effects. We assume that $G_i = G_T - G$ by conservation. Active RhoA results in cell contraction, which reduces tension. Tension is assumed to increase the activation rate of RhoA. (B) A resting cell (rest length L_0 , top left) is stretched by an external force to length L (bottom left); the ‘spring’ schematic represents contractile actomyosin. Tension $T \propto (L - L_0)$ in the stretched cell activates RhoA (inset, lower right, color scheme as in (A)), leading to a coupled mechanochemical system. RhoA activity results in actomyosin-powered cell contraction, reducing cell tension. As RhoA is inactivated by the loss of tension (upper right), the cell relaxes. (C) Mechanical representation of the actomyosin cell cortex as a Kelvin–Voigt element.

a length L as shown in figure 1(C). A cell at mechanical equilibrium has some constant ‘rest-length’, $L = L_0$, as in figure 1(B). To couple the signaling with the mechanical tension, we assume that cell tension, T , proportional to $(L - L_0)$, enhances RhoA activation. Thus, if a resting cell is stretched, RhoA activity increases. In turn, active RhoA results in contraction of the cell (we assume that active RhoA decreases the rest-length of the cell). As the cell contracts, it counteracts the stretching force, resolving the tension. This reduces the GTPase activity to a lower level. The overall paradigm of the model is shown as a cycle through states following the purple arrows in figure 1(B).

2.1. Model equations and definitions

For the activity of the GTPase, we adopt the generic equation

$$\frac{dG}{dt} = (\text{Tension-dependent rate of activation}) G_i - (\text{Rate of inactivation}) G, \quad (2.1)$$

where G_i is the level of inactive GTPase. Ignoring spatial variation, and assuming that the total GTPase G_T is roughly constant over the timescale of interest ($G_T = G + G_i = \text{constant}$), leads to a single equation, (2.1) with $G_i = G_T - G$. This equation is a direct adaptation of the 1-GTPase spatially-uniform version of the model in [39], with the addition of the mechanical coupling.

In the case of a linear equation (2.1), that is, if terms in braces are constant, no interesting behavior is found. Some feedback is needed to obtain the nonlinearities that generate bistability and allow for non-trivial dynamics. We have typically assumed positive feedback from active GTPase to its own activation

[5, 39] (see [40] for the equivalence of other assumptions). Furthermore, based on the prevalence of GEF-associated mechanotransduction [17], we include the tension-dependent feedback $f(T)$ in the activation rate. This leads to a model of the form

$$\frac{dG}{dt} = \left(b + f(T) + \gamma \frac{G^n}{1 + G^n} \right) (G_T - G) - G, \quad (2.2a)$$

where b is basal activation rate (scaled by the constant inactivation rate), and γ is a similarly scaled rate of feedback activation. (Details of the scaling are provided in the appendix.) In our model, cell tension depends on the ‘size’ L of the cell relative to its concurrent rest-length L_0 . We considered several forms of $f(T)$, as described in the appendix. Here we concentrate on the case that

$$f(T) = \beta \frac{1}{1 + \exp[-\alpha(L - L_0)]}, \quad \text{where} \quad T = L - L_0. \quad (2.2b)$$

The parameter β governs the strength of feedback from tension to GTPase activation. The ‘squashing function’ in (2.2b) means that the mechanical input has no effect if $L \ll L_0$, but builds up to a maximal level of β for $L \gg L_0$. Consequently, our ‘model GTPase’ is sensitive to a pulling force, but not to a squeezing or contractile force. (It is straightforward to generalize this minimal assumption.) The parameter α governs the sharpness of the GTPase activation response to cell stretching. It is worth remarking that this form of mechanical model (2.2a) with (2.2b) bears a close resemblance to the equation proposed in [15] for the dynamics of active RhoA in human fibrosarcoma cells that are exposed to mechanical tension. Our squashing function has the same basic property of switch-like activation as their Hill-function dependence on T .

For the mechanical coupling, we assume that GTPase activity (e.g. RhoA activating ROCK, which activates myosin light chain) effectively shortens the rest length of the ‘cortical actomyosin spring’ promoting contraction. We model this by the following equation for the cell size L :

$$\frac{dL}{dt} = -\varepsilon(L - L_0), \quad \text{where} \quad L_0 = \ell_0 - \phi \frac{G^p}{G_h^p + G^p}, \quad (2.2c)$$

and $\varepsilon = 2k/\lambda$ is the rate of contraction. This model assumes that the cell acts as an overdamped elastic spring with Hookian spring constant k , and viscous coupling to a fixed substrate (viscosity λ). The rest length, L_0 , is assumed to decrease from a fixed rest length, ℓ_0 , depending on the amount of active GTPase within the cell, G . The dependence on G is represented by a Hill function with amplitude ϕ , half-maximum GTPase activity G_h , and power p . For large GTPase activity G , the rest length approaches $L_0 \approx \ell_0 - \phi$, while for low GTPase activity, the rest length remains near ℓ_0 . A switch occurs close to the activity level $G = G_h$. The larger the value of p , the sharper the transition between small and large L_0 values. Equation (2.2c) presumes the overdamped regime, where inertial forces are negligible, as appropriate for modelling cell-scale behavior. Equation (2.2c) follows from a force balance at the two cell ends:

$$\lambda \frac{dx_1}{dt} = k(L - L_0) \quad \text{and} \quad \lambda \frac{dx_2}{dt} = -k(L - L_0), \\ \text{where } L = x_2 - x_1, \quad (2.3)$$

for x_1, x_2 positions of the left and right cell boundaries (in 1D), and from $\frac{dL}{dt} = \frac{dx_2}{dt} - \frac{dx_1}{dt}$.

2.2. Results

The single GTPase model on its own (with $\beta = 0$), is bistable for a range of parameters. As the basal activation rate b increases, the system transitions from a monostable state with low GTPase activity, through a bistable regime, and finally to a monostable state with high GTPase activity (figure 2(A) and [29, 39]). With mechanical feedback ($\beta \neq 0$) as described in section 2.1, we find three regimes of behavior: (1) for small β , the cell remains relaxed with low GTPase activity, (2) for large β , the cell becomes contracted with high GTPase activity, and (3) for intermediate β , the cell dynamics tends to a stable limit cycle with GTPase activity cycling between low and high levels. The bifurcation diagram of figure 2(B) shows these three regimes of behavior, displaying steady state cell length, L , as a function of the coupling feedback strength, β . For this choice of parameters, the three regimes of behavior occur for different intervals of β ; however, for different parameter values, it is possible that the limit cycle and contracted steady-state can both be stable for the same value of β .

The dynamics of the cell size (L , solid), rest-length (L_0 , dash-dotted curve) and GTPase activity (G , dashed

curve) is shown in figure 3 for each of these regimes. When the feedback from tension upon GTPase activation is small, (A) $\beta = 0.05$, the cell remains relaxed. As the feedback parameter increases, (B) $\beta = 0.2$, the cell oscillates, or (C) for $\beta = 0.3$, the cell contracts and maintains a small length.

We can understand the results based on known dynamical systems behavior of a bistable system (the GTPase activity) with slow negative feedback (the mechanical contraction). The coupling can constrain the bistable system to either its low or its high steady state levels, or, for intermediate coupling, lead to a trajectory around a hysteresis loop. In the latter case, the system behaves as a relaxation oscillator. As shown by the hysteresis loop in figure 2(A), a given value of the activation rate b is increased when the cell is stretched, eventually leading to a transition from low to high GTPase activity. At this point, the GTPase activity leads to cell contraction, effectively decreasing the rest length L_0 . As the cell contracts, L approaches L_0 , and tension decreases, reducing GTPase activation rate and transiting to the low GTPase state. This resets the rest-length to a larger value. With the appropriate relative timescales of mechanics and chemical signaling, this cycle repeats, setting up the limit cycle oscillations.

3. Mechanical coupling in a 1D array of cells

Having characterized the minimal ‘model cell’, we next considered the behavior of a coupled array of such cells. As a first step, we coupled cells mechanically in one spatial dimension (1D), as shown in figure 4. Here the lengths of the cortical actomyosin Kelvin elements are simply the distances $L_j = x_{j+1} - x_j$, $j = 1, \dots, N - 1$ between ‘nodes’ (edges of cells along a 1D axis). Each cell has its own internal GTPase signaling, following equation (2.2a), and only responds to neighboring cells through mechanical force. Hence, we assumed that the motion of the cell ends, x_j , is prescribed by the following system of ODEs:

$$\lambda \frac{dx_1}{dt} = k(L_1 - L_{1,0}), \quad (3.1a)$$

$$\lambda \frac{dx_j}{dt} = -k(L_{j-1} - L_{j-1,0}) + k(L_j - L_{j,0}), \quad (3.1b)$$

$$\lambda \frac{dx_N}{dt} = -k(L_{N-1} - L_{N-1,0}), \quad (3.1c)$$

with $j = 2, \dots, N - 1$. The rest-length in each cell, $L_{j,0}$, is coupled to GTPase signaling according to equation (2.2c).

3.1. Tissue dynamics in 1D depend on mechanical feedback strength

When many cells are coupled together, new tissue-level behaviors emerge. For example, as one cell is displaced

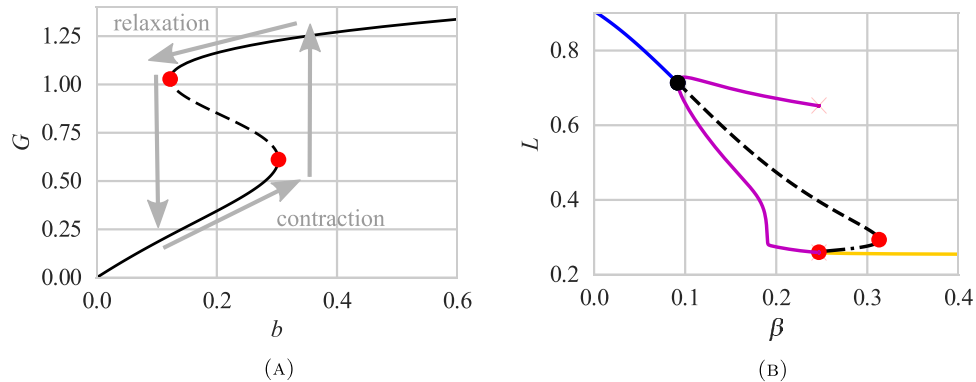


Figure 2. Bifurcation diagrams for the minimal model (2.2). (A) On its own the GTPase model (2.2a) (with $f(T) = 0$) exhibits bistability with respect to the activation rate b . (Other parameters: $\gamma = 1.75, n = 4, G_T = 2$). Mechanical tension affects the GTPase activation rate, leading to the possibility of a relaxation oscillator (hysteresis loop) shown in this diagram. (B) Bifurcation diagram for the coupled GTPase-tension minimal model equation (2.2), showing how cell length L varies with the strength of coupling (β) of tension to GTPase activation. L can be long (small β , solid yellow line), oscillatory (middle values of β , magenta line), or short (large β , solid blue line). In both panels, red points are saddle node bifurcations, and the black point corresponds to a Hopf bifurcation. Other parameters are $b = 0.1, \gamma = 1.5, G_T = 2, \beta = 0.2, \ell_0 = 1, \phi = 0.75, G_h = 0.3, \varepsilon = 0.1, \alpha = 10$, and $n = p = 4$.

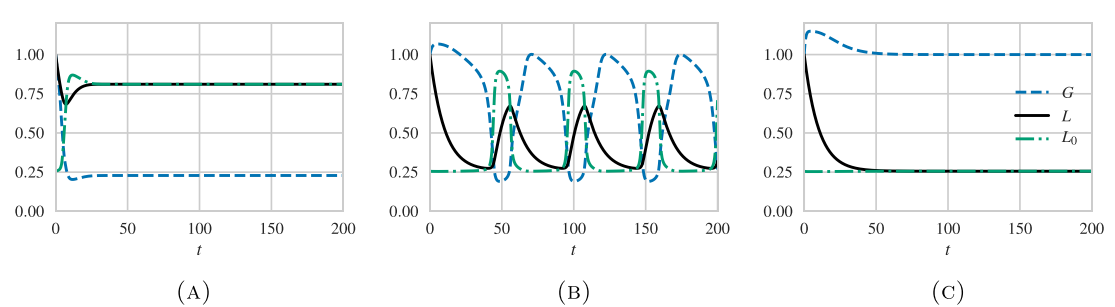


Figure 3. Dynamics of the minimal model for a single cell with one GTPase ('RhoA') and feedback from tension to GTPase activation, equation (2.2). In (A), the feedback from tension ($\beta = 0.05$) is weak, and the cell remains relaxed. In (B), the feedback ($\beta = 0.2$) is of intermediate strength, and limit cycle oscillations arise. In (C), the coupling is so strong ($\beta = 0.3$) that GTPase activity is always high, and the cell stays in a contracted state. Parameters are $b = 0.1, \alpha = 10, \gamma = 1.5, n = p = 4, \ell_0 = 1, G_T = 2, \phi = 0.75, G_h = 0.3, \varepsilon = 0.1$. When the GTPase activity level is close to $G = G_h$, the cell rest length changes sharply from $L_0 \approx \ell_0$ to $L_0 \approx \ell_0 - \phi$ (green dash-dotted), resulting in the dramatic changes in cell length seen in (B). Some lag stems from the slower dynamics of L , due to the slow mechanical response (small parameter ε).

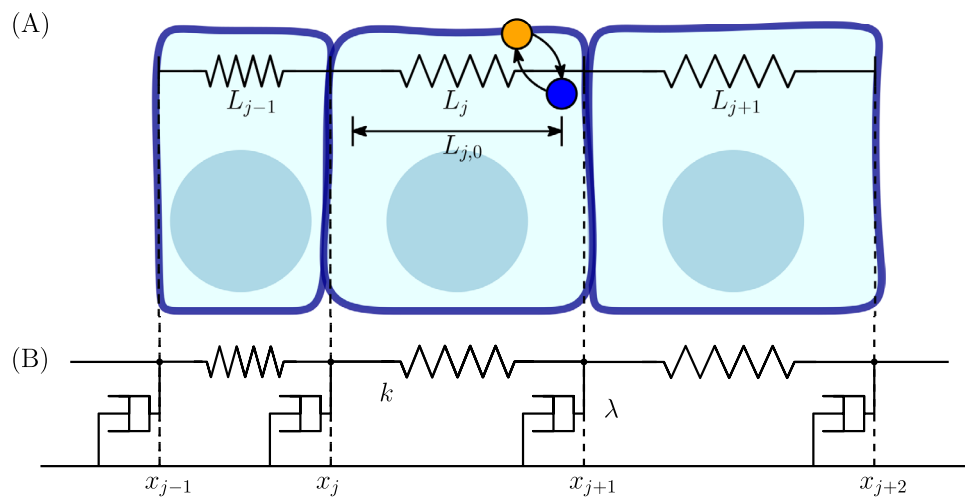


Figure 4. Cell interactions in a 1D array of 'model cells'. (A) The contraction-relaxation of each cell affects the force of pulling on its neighbors. Each cell has its own internal GTPase signaling. (B) The array behaves much like a system of overdamped springs in series. The GTPase signaling affects the rest-lengths of the springs L_j , and the dynamics then moves the nodes x_j that represent cell borders.

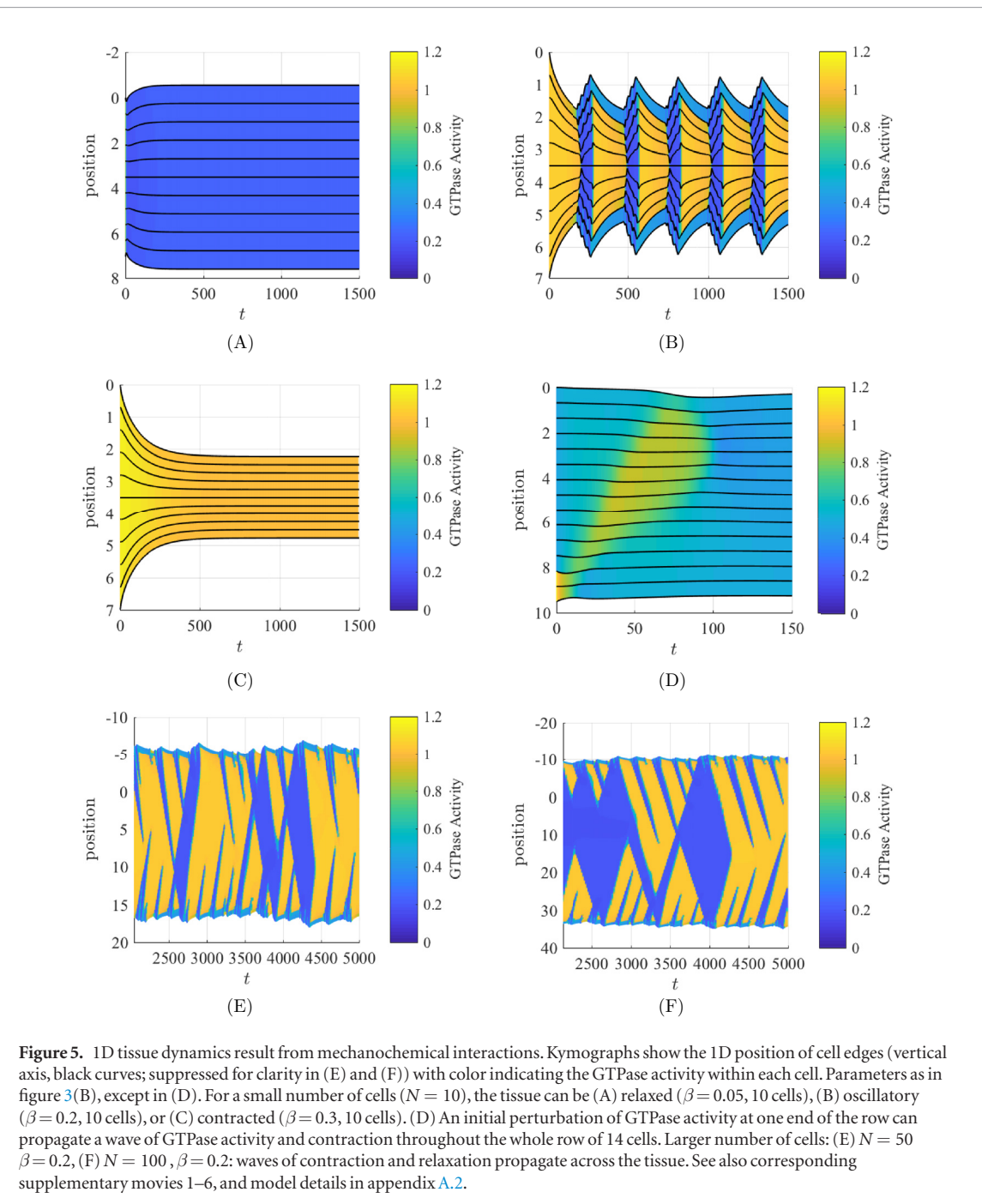


Figure 5. 1D tissue dynamics result from mechanochemical interactions. Kymographs show the 1D position of cell edges (vertical axis, black curves; suppressed for clarity in (E) and (F)) with color indicating the GTPase activity within each cell. Parameters as in figure 3(B), except in (D). For a small number of cells ($N = 10$), the tissue can be (A) relaxed ($\beta = 0.05$, 10 cells), (B) oscillatory ($\beta = 0.2$, 10 cells), or (C) contracted ($\beta = 0.3$, 10 cells). (D) An initial perturbation of GTPase activity at one end of the row can propagate a wave of GTPase activity and contraction throughout the whole row of 14 cells. Larger number of cells: (E) $N = 50$ $\beta = 0.2$, (F) $N = 100$, $\beta = 0.2$: waves of contraction and relaxation propagate across the tissue. See also corresponding supplementary movies 1–6, and model details in appendix A.2.

or contracts, its neighbors are stretched or squeezed. This change in length then affects tension, T , and ultimately the GTPase activity, G of the neighbor(s), that can similarly affect their neighbors, and so on. The emergent behavior depends on the signaling parameters of the individual cells. For example, if the strength of feedback from mechanics to GTPase activity, β , is sufficiently small or sufficiently large everywhere, the entire tissue will be relaxed (and long) or highly contracted (and short), respectively. Examples of these behaviors are shown in figures 5(A) and (C) and in supplementary movies 1 and 3 (stacks.iop.org/PhysBio/15/046004/mmedia).

For β in the (single-cell) oscillatory regime ($\beta = 0.2$, as in figure 3(B)), and a small array of cells ($N = 10$), the entire array can exhibit synchronous

oscillations, as shown in figure 5(B) and in supplementary movie 2. In this case, as each cell expands or contracts, the force exerted on its nearest neighbors induces a change in the chemical signaling, which results in the coordination of the entire group (possibly excluding the cells at either end). This shows up as coherent bands of color in figure 5(B) while the total length of the array (vertical dimension in figure 5) oscillates.

In figure 5(D), two cells at the right end of the row are initially ‘stimulated’ with high GTPase activity, while the rest of the cells are at their relaxed steady-state. Contraction of the stimulated cells stretches their immediate neighbors to the left, which activates new GTPase signaling in those neighbors and subsequent contraction. In this way, a unidirectional wave

of GTPase activity and contraction sweeps across the entire row of cells. (See appendix A.2 for parameter and model details.) As we comment in the Discussion, this wave of contraction resembles a wave associated with zippering in the neural tube closure of an ascidian embryo [41].

As the number of cells increases, the spatial extent of the mechanical force transduction can no longer span the entire ‘tissue’, and appears to become localized to some neighborhoods. Then, patches of contraction and relaxation emerge; these can propagate throughout the tissue as waves of contraction-relaxation. Typical examples for 50 and 100 cells in such 1D arrays are shown in figures 5(E) and (F) and in supplementary movies 5 and 6. In such large arrays, GTPase activity is also seen to form wave patterns that sweep back and forth across the 1D domain. This leads to the slanted bands of color in figures 5(E) and (F). Even though the GTPase activity is not directly coupled between cells, the mechanical coupling effectively leads to GTPase coordination on some spatial and temporal scale.

While we cannot claim to have exhaustively explored all possible behaviors of this 1D cell collective, the few results shown here demonstrate an interesting range of behavior. Studying this phenomenon in single cells and in a 1D array of cells, so far, has drawbacks in missing the representation of cell shape and interactions with more than two neighbors. Consequently, we next consider realization of the same idea in a 2D setting.

4. Cell shape and cell–cell interactions in 2D epithelial sheets

4.1. Adapting the model

In order to describe cell expansion and/or contraction in 2D, we modified the model to represent changes in projected cell area, A , rather than cell length. Generalizing from the 1D model, we assign a ‘resting cell area’ A_0 to the cell, and assume that positive ($A - A_0$) corresponds to an average cell-stretching tension that has an effect in 2D similar to ($L - L_0$) in the 1D model cell. (This assumption can be modified, scaled according to $A \approx cL^2$, or adapted to experimental data). In the context of the simple toy-model, the main effect, preserved by these assumptions, is that GTPase activity and mechanical tension switch one another on or off.

To simulate cell shape and intracellular chemistry, we used a publicly available software package, CompuCell3D that represents cell shapes using the cellular Potts model (CPM) formalism [42]. Briefly, the pixel-based motion of a cell edge outwards (expansion) or inwards (contraction) is governed by a Hamiltonian, \mathcal{H} , describing the total energy in the system. The Hamiltonian includes adhesion energies, and ‘volume’ constraints (area constraint in 2D). At each time step in the simulation, several small changes are introduced

(pixel-copy attempts or spin-copy attempts). The CPM algorithm accepts such changes if this decreases the Hamiltonian (overall ‘energy’ of the system), or accepts it randomly otherwise as a small noise-induced ‘fluctuation’. While CPM does not explicitly track forces, it has recently been shown to be consistent with other simulations where forces are made explicit [43], for example, vertex-based cell models.

Several aspects of the simulations were adapted to the technical requirements of the CPM. Time was scaled by a factor τ , and the notion of a ‘target area’, A_T , was introduced (details in the appendix). The actual cell area A and the GTPase-governed target cell area A_T are tracked in each CPM cell. The time constant τ scales ‘real time’ to Monte Carlo step (MCS) ‘time’. As before, we ignore spatial variation in GTPase activity within a cell, and assume that the total GTPase, G_T , is roughly constant over the timescale of interest. The GTPase and target area dynamics are prescribed by ODEs within each cell, while the actual cell area, A , is updated stochastically to approach the target area A_T by the CPM. As before, we assume that increasing tension (represented as the difference between target area and actual cell area), can increase GTPase activity via the function $f(T)$. We first examined the GTPase-tension model in a single 2-dimensional cell, and later consider the coupling between interconnected cells.

4.2. Single cell dynamics

With appropriate calibration, we found that the 2D CPM implementation recapitulates the behavior found in the single cell model. As shown in figures 6(A) and A10, a parameter set corresponding to 1D cell oscillations also led to single-cell oscillations in the 2D CPM cell. The CPM also produces relaxed cells and contracted cells for corresponding parameter sets in the 1D model, see figures A8 and A9 for relaxed cells.

CPM simulations have inherently stochastic behavior due to the allowable random fluctuations mentioned above. As a result, we discovered new behavior that was not found in the deterministic 1D cell simulations, namely that spontaneous cycles of high to low GTPase level (and low to high cell areas) could occur, even in parameter sets consistent with monostable states. An example of this type is shown in figure 6(B). Here, parameter values were set to the stable small-size single-cell regime in the 1D model ($\beta = 0.5$). The cell was in a contracted state for some time, but displayed two cycles of contraction-relaxation, at MCS 100 and 150, before returning to its quasi-quiescent state. In figure A11, we also see an example of cells switching between small and large limit cycle oscillations for $\beta = 0.175$.

4.3. Coupling CPM cells in 2D

We asked what happens when there are multiple cells in the 2D simulation. Accordingly, we set up two types of situations in which N cells are present, each governed by its own set of 2D equations (see appendix)

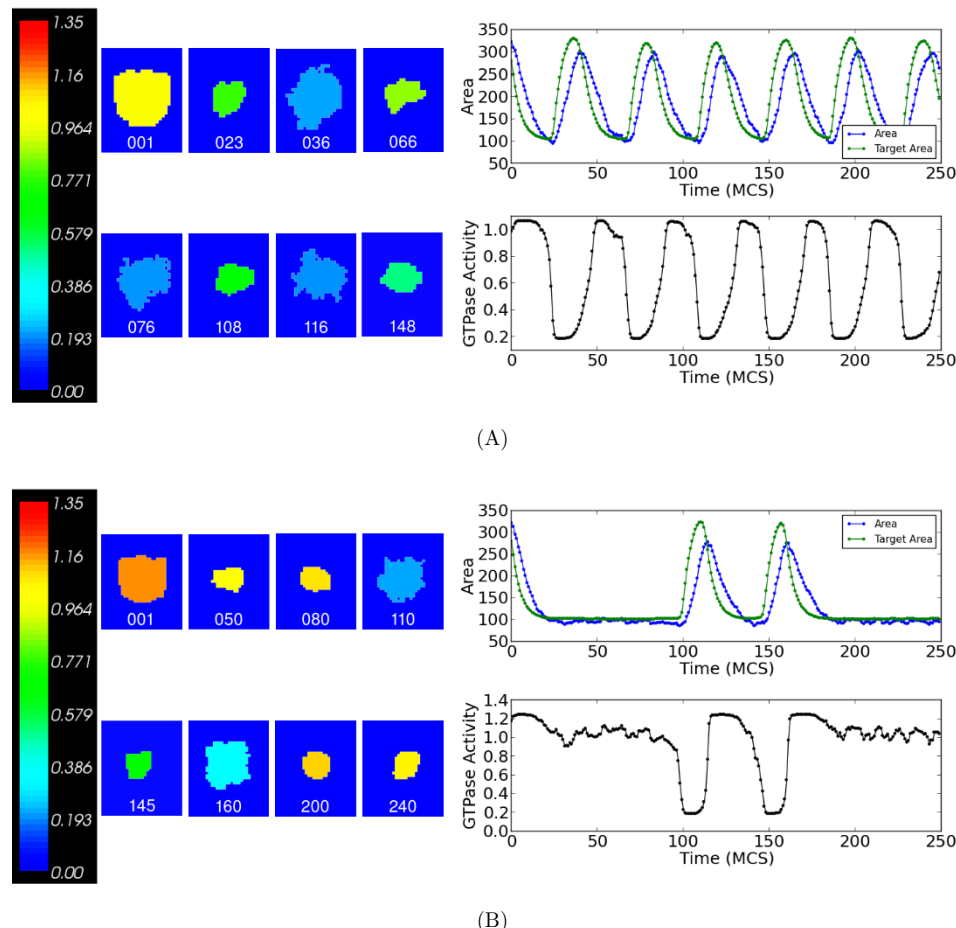


Figure 6. Single cell oscillations in 2D cells simulated with the cellular Potts model (CPM) formalism using the CompuCell 3D software [42]. In (A) and (B), cell color represents a (spatially uniform) GTPase activity level from low (blue) to high (yellow and orange), as shown in the color bar. Cell shape changes over time as indicated by the progression of snapshots numbered by the Monte-Carlo steps (MCS) of the CPM (MCS increase left to right and top to bottom). Cell target area (green) and actual area (blue) as well as GTPase activity is plotted over 250 MCS of the CPM. In (A), $\beta = 0.2$ results in a single oscillatory cell. In (B), the cell stochastically switches between high GTPase steady state (corresponding to $\beta = 0.5$) and a large amplitude limit cycle. Other parameters were: $\tau = 2000$, $b = 0.1$, $m = 10$, $\gamma = 1.5$, $n = p = 4$, $G_T = 2$, $\varepsilon = 0.1$, $a_0 = 400$, $\phi = 0.75$, and $G_h = 0.3$.

with the same set of parameters but random initial conditions. As shown in figure A2 for $N = 9$ cells, our first implementation was of cells that have no direct mechanical coupling. As expected, in this case, cells behave independently with distinct and uncorrelated copies of the dynamics. The Rho GTPase levels inside such cells (top, figure A3) remain unsynchronized, as detected by the Kuramoto order parameter and the variance in the phase (details in appendix A.4).

We next initiated cells that were contiguous and implemented cell-cell interactions via adhesion terms in the CPM Hamiltonian (details in appendix A.3). Essentially, cells that have larger interfaces with their neighbors have stronger adhesion (and lower adhesion energy). An example of such simulations are shown in figure A4. As a cell changes size, neighboring cells are affected through cell-cell adhesion. As one cell area contracts, its neighbors are stretched, causing their tension, proportional to $(A - A_T)$, to increase. This promotes a neighbor's GTPase activity, and leads it to contract. In this way, mechanical forces are propagated throughout the tissue and affect GTPase signaling in

each cell. As seen in figure A5, GTPase activities rapidly synchronize in the entire group of nine cells, with a few small fluctuations in phase seen occasionally. The larger Kuramoto order parameter and lower variance in the phase (note scaling on the vertical axis) as compared with simulation for independent cells figure A3 also confirms this synchronization.

We experimented with the adhesion between cells, which essentially couples neighbors to one another. As shown in the sequence of figures A5–A7, as cells become more adhesive to one another ('low cell-cell adhesion energy') than to the surrounding 'medium', the mechanical coupling is stronger, and the synchronization of cell oscillations is more regular.

4.4. Waves of contraction and GTPase activities in 2D model tissue

Next, we asked how larger numbers of cells, also in 2D CPM, would behave when coupled mechanically through their adhesion. To probe this question, we simulated a circular tissue composed of 373 contiguous cells with initial areas randomly chosen.

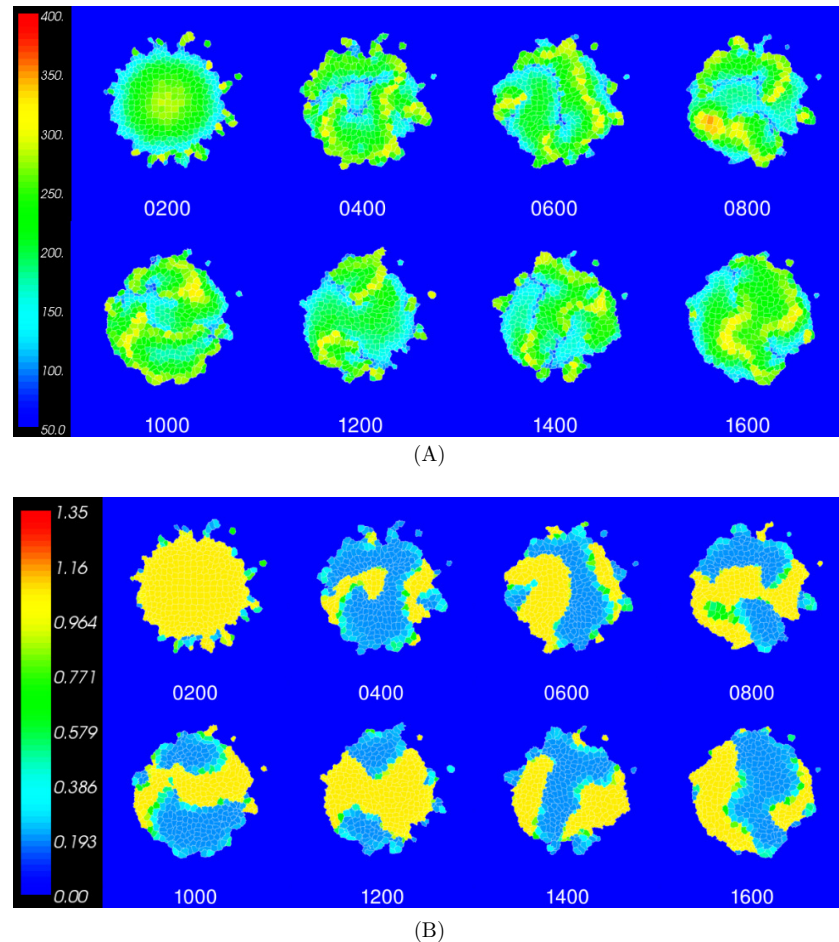


Figure 7. Simulation of a 2D ‘tissue’ ($N = 373$ cells) in the intermediate adhesion scenario using CompuCell3D [42]. Individual cells satisfy the minimal GTPase-tension model, with $T \propto (A - A_T)$, where A is cell area, and A_T is the target area. Cell-medium adhesion energy (80) is equal to cell–cell adhesion energy (80) in the Hamiltonian, \mathcal{H} . In (A), cells are colored based on their current cell area, while in (B), cells are colored based on the uniform level of GTPase activity within each cell. Cells with smallest area (dark blue in (A)) are correlated with an interface between high (orange) and low (blue) GTPase activity in (B). Waves of contracting cells and relaxing cells are observed throughout patches in the tissue. See supplementary movies 7A and 7B. Parameters listed in appendix A.3 and A.5.

As before, we chose parameters in the oscillatory single-cell regime. Results are shown in figure 7 for the case of intermediate adhesion, in figure 8 for the case of strong adhesion, and in figure A12 for the case of weak adhesion (see also supplementary movies 7A and 7B, 8A and 8B, and 12, respectively). Here the 2D tissue is much larger than a few cell diameters. In figures 7 and 8, we show two views of the same ‘tissue’, one (A) indicating cell area on a color scheme of blue (small) to yellow (large), and a second (B) representing the concurrent GTPase activity level from low (blue) to high (orange).

In contrast to the case of few cells, where synchronized oscillations were observed over the entire population, we found that in the larger tissue, synchronization is limited to patches. We found that waves of contraction/relaxation and GTPase activity propagate throughout the tissue. This behavior can be seen in the successive snapshots in figures 7(A) and (B) and in supplementary movies 7A and 7B for the case of intermediate cell–cell adhesion. Bands of highly contracted cells (dark blue) are noteworthy in several panels in figure 7 (A), and coincides with

interfaces between zones of high and low GTPase activity in figure 7(B).

The strength of cell–cell adhesion affects the strength of coupling and extent of synchronization. In the case of weak cell–cell adhesion (figures A12(A) and (B) and supplementary movies 12A and 12B), relatively small patches are seen, and cells tend to detach from the periphery of the tissue. Waves of contraction and expansion are observed. As cell–cell adhesion is increased from the baseline simulation in figure 7, cells are more likely to favor adhering to each other. They then experience larger changes in area as one of their neighbors shrinks or grows. This results in nearly the entire tissue of cells expanding and contracting, though we still tend to see a wave of synchronization spreading from the center to the edge of the tissue, as in figure 8 and supplementary movie 8A. We conjecture that the patch size (number of cells in a group with coordinated behavior) increases with the strength of cell–cell adhesion.

In our final CPM experiment, we considered the case that cells are heterogeneous, with a range of val-

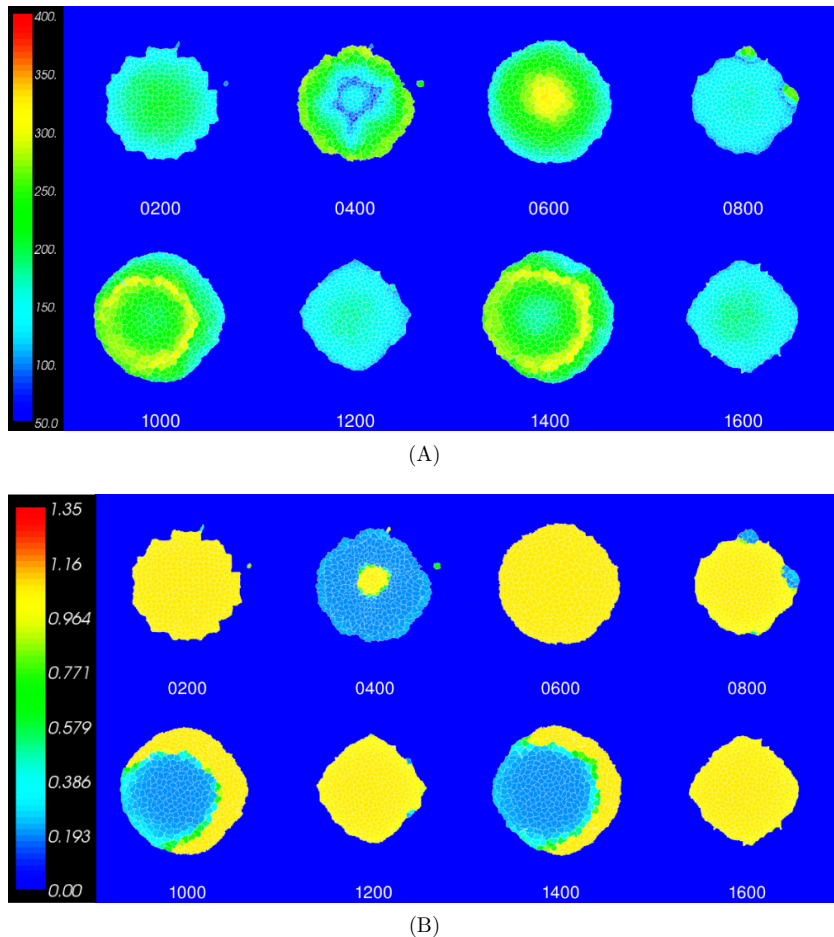


Figure 8. As in figure 7 but for the strong adhesion scenario. Cell–medium adhesion energy (80) is greater than cell–cell adhesion energy (30) in the Hamiltonian, \mathcal{H} . The entire tissue is synchronized. In (A), cells are colored by area, while in (B), cells are colored by GTPase activity. Notice that cells at the outer edge are first to expand/contract as they are less constrained by neighbors, so that expansion/contraction is ‘outside-in’. See supplementary movies 8A and 8B. Parameters are the same as in figure 7, and are listed in appendix A.3 and A.5.

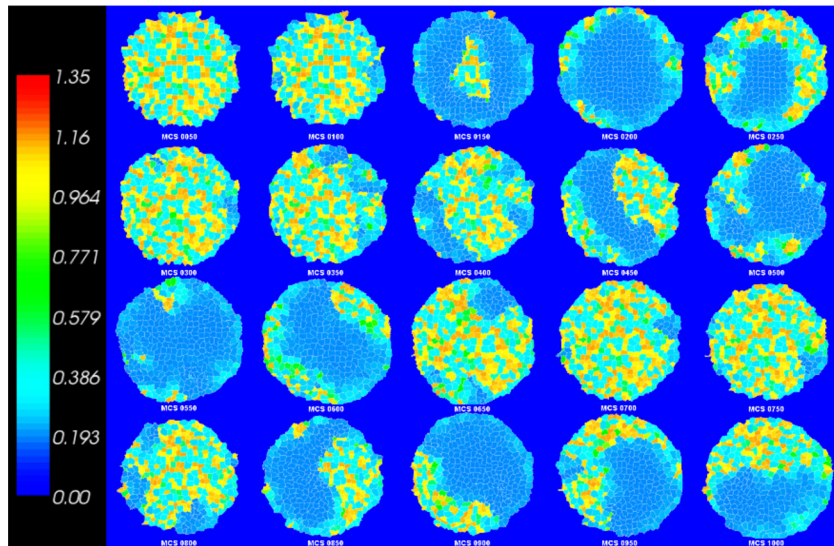
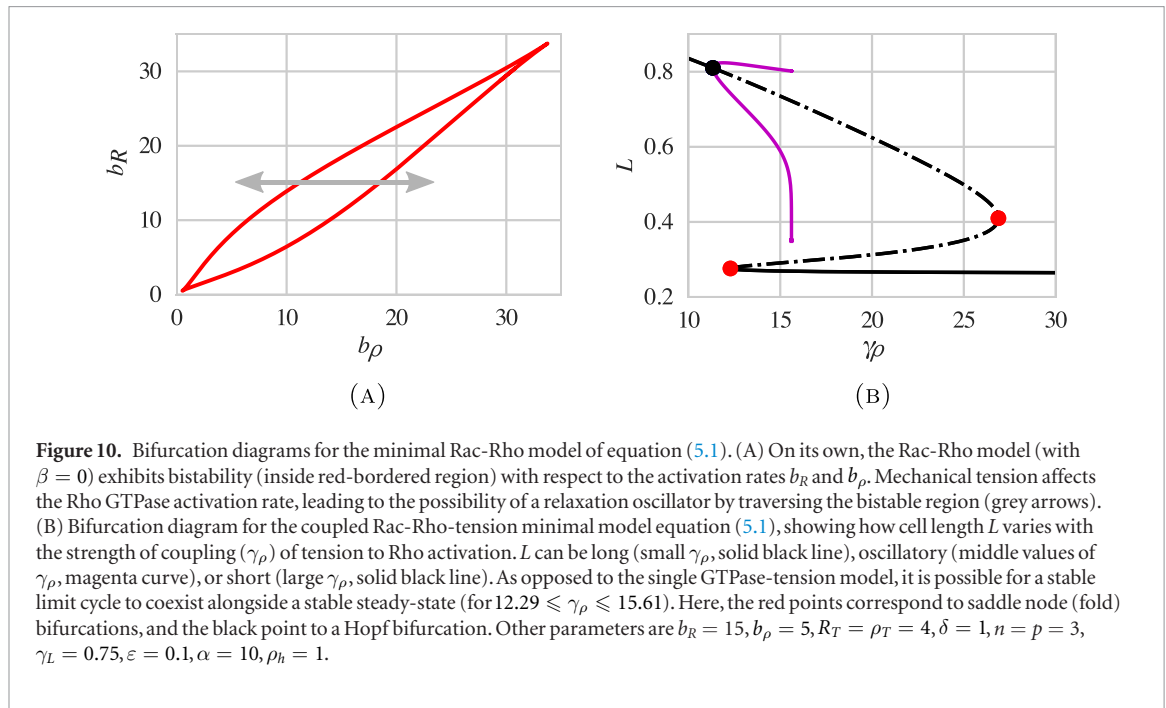


Figure 9. As in figure 7(B), but with the parameter β (feedback strength from tension to GTPase activation) randomly chosen for each cell. Cells are colored by GTPase activity. Cells in steady state are forced to oscillate due to mechanical coupling with cells that are in the limit cycle regime. In this case, the baseline area parameter is increased to $a_0 = 600$ (resulting in larger variation in cell area), and temperature parameter of Potts model $T = 15$ is decreased from baseline. In the Hamiltonian, \mathcal{H} , cell–cell adhesion energy is 60, and cell–medium adhesion energy is 80. Other parameters are as in appendix A.3 and A.5. See supplementary movie 9.



ues of the feedback parameter β coupling mechanics to the GTPase activation. We simulated a large tissue, as before, but assigned randomly chosen values of β to the cells. Results are shown in figure 9 and supplementary movie 9. With the range of values of β , individual cells could be either contracted, oscillatory, or relaxed. Due to the presence of some oscillatory cells in the tissue, those cells which would normally be quiescent at either relaxed or contracted steady-states, undergo oscillations due to pulling by oscillatory neighbors. We see patches of activity in the tissue that persist, though with a heterogenous GTPase activity. These forced oscillations are suggestive of a mechanism by which tissue dynamics can be driven by a few pace-maker cells, whose phenotype is oscillatory.

5. Rac and Rho GTPase model

We asked whether some of the lessons learned in our single-GTPase model would carry over to similar conclusions in a slightly expanded Rac-Rho GTPase circuit. It is well-known that Rac1 and RhoA are mutually inhibitory under many situations [31,33,37]. Our analysis derives from the well-mixed variants of the Rac-Rho model described in [39], and in the melanoma-based modeling of [29]. In the latter case, coupling of front and rear compartments of a cell (through extracellular matrix signaling) was found to lead to the possibility of distinct behavioral regimes, including stable high Rho or Rac, or cycling between those levels. (Here the mechanical coupling has an effect similar to the ECM coupling in that paper.)

In the mutually inhibitory Rac-Rho model, the total level of Rac (Rho) GTPase, R_T (ρ_T) is assumed to be roughly constant over the timescale of interest. Hence only the active forms of the GTPases need to be tracked. Assuming that each of Rho and Rac inhibits

the activation of the other, we adopted the set of equations,

$$\frac{dR}{dt} = \frac{b_R}{1 + \rho^n} (R_T - R) - \delta R, \quad (5.1a)$$

$$\frac{d\rho}{dt} = (b_\rho + f(T)) \frac{1}{1 + R^n} (\rho_T - \rho) - \rho, \quad (5.1b)$$

where $f(T)$ represents the activation of Rho GTPase by tension T .

Here we kept the assumption that Rho GTPase activity leads to cell contraction and the buildup of tension T , as before. Model equations and details are gathered in appendix A.7.

On its own, without feedback from mechanics, the minimal Rac-Rho mutual inhibition model has a region of bistability, as shown in figure 10(A). As either the basal activation rates, b_ρ or b_R , increase, the system transitions from a monostable state with either species at a high steady-state (and the other at a low steady-state) or from a coexistence state, into the bistable regime. We assumed, as before, that stretching a cell would increase the activation rate of RhoA. With that assumption, we find the same regimes of behavior as in the single GTPase model section 2.1. These three regimes of behavior depend on the strength of feedback from tension to Rho activation (a parameter denoted γ_ρ). The dependence is shown in the bifurcation diagram in figure 10(B). For small γ_ρ , the cell remains long and relaxed, with high levels of Rac activity and low levels of Rho activity figure 11(A). For large γ_ρ , the cell is contracted, (small L) with low levels of Rac activity and high levels of Rho activity as shown in figure 11(C). For intermediate γ_ρ , limit cycle oscillations arise as in figure 11(B). There is a regime of parameter space where a stable limit cycle and stable steady-state coexist (approx-

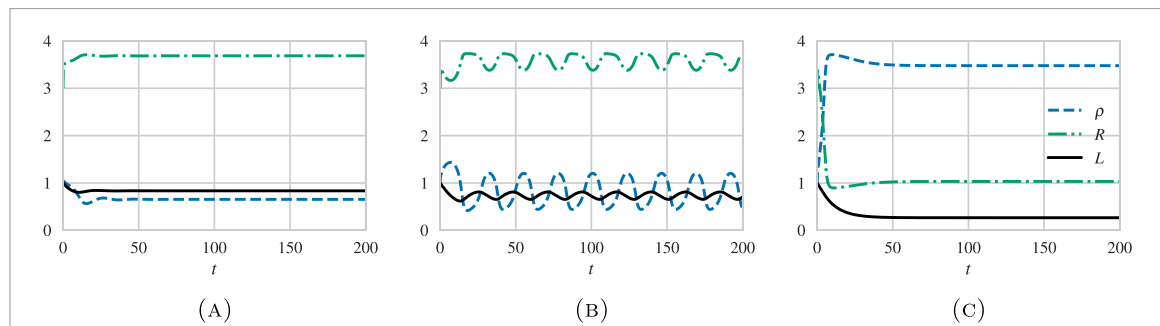


Figure 11. Dynamics of the model for a single cell with two GTPases ('Rac1' and 'RhoA') and feedback from tension to Rho activation. In (A), the feedback from tension ($\gamma_\rho = 10$) is weak, and the cell remains large and relaxed ($L \approx 1$) with high Rac and low Rho activities. In (B), the feedback ($\gamma_\rho = 14$) is of intermediate strength, and limit cycle oscillations arise, provided that the initial conditions send the system to the stable limit cycle, instead of the contracted-cell steady-state (see figure 10). In (C), the coupling is so strong ($\gamma_\rho = 18$) that RhoA activity is always high, Rac is low, and the cell stays in a contracted state ($L \ll 1$). Parameters are as in figure 10.

mately $12.29 \leq \gamma_\rho \leq 15.61$). In this parameter regime, depending on initial conditions, the cell may either end up in the oscillatory regime, or at the contracted cell state.

In the above Rac-Rho model, we considered only coupling between mechanical tension and Rho activity, ignoring possible direct effects of mechanosensing on Rac activity. Rac is known to cause cell spreading via WASP/Arp2/3-based actin assembly, an effect that we had similarly omitted. To check the possible outcomes of such additional factors, we briefly explored several variants of the above default Rac-Rho-tension model. Specifically, we experimented with inclusion of (1) the effects of compression (as opposed to tension) sensing with feedback to Rac activation and (2) the effect of Rac activity on cell size, modeled as an increase in the rest-length L_0 . Feedback from mechanics to Rac activation can be interpreted as a change in b_R in figure 10(A). This can push the underlying Rac-Rho signaling model into a regime of different behaviour—high Rac, bistability, coexistence, or low Rac—and alter the resulting cell behaviour accordingly (in a mechanical feedback-dependent manner). We observed behaviour similar to figure 11; albeit with Rac activity increasing the cell length and the relaxation oscillation arising from compression instead of tension.

Aside from the above complementary Rac-feedback-only model, we also experimented with mixed Rac and Rho feedbacks and antagonistic effects on cell size. We also considered feedback from tension and/or compression to GAPs as well as GEFs (inactivation versus activation terms in the GTPase equations). Overall, similar regimes of behaviour can be found in many such examples, within smaller or larger regions of parameter space. Cases of specific interest should henceforth be linked to specific biological examples where the mechanical coupling to known GEFs or GAPs is of interest.

6. Discussion

Feedback between biochemical signaling and mechanical forces plays a vital role in developmental

biology and morphogenesis. A recent review [44] is complementary to our investigation, highlighting how diffusion-driven patterns, differential adhesion, buckling instabilities in growing layers, and flows in active materials (cytoskeleton and motor proteins) lead to patterning. Following the experimental work of [14], a single-cell model was also developed to describe the inhibition of cell polarization by membrane tension [45]. The authors used a more sophisticated spatio-temporal model of the GTPases in a 2D cell (based on the idea of wave-pining [5]), its downstream effect on actin, and a cell boundary represented using the phase-field method. The model accounted for observations on how build-up of tension in a neutrophil (by aspiration into a micropipette) and sudden release of tension (by severing a long cellular protrusion) affect the level and distribution of GTPase activity.

While the effect of tension on GTPase activity was studied previously [14, 15], to our knowledge, this is the first model that links GTPase-induced cell contraction to tension-induced GTPase activity in single cells and in a 1D and 2D tissue. Interestingly, a model based on mechanochemical coupling of some (indeterminate) signaling chemical and cell length that was studied mathematically and computationally decades ago [25] bears striking resemblance to our own. That previous model was aimed at understanding folding and invagination of epithelia, for example in the process of gastrulation [26, 27]. It was shown then that a localized stimulus in one cell could result in active localized contraction in some neighborhood, creating the first fold in an early embryo. As GTPases and their effects were yet to be characterized, this predecessor in the 1980s was theoretical, ahead of its time, and visionary. We have Odell and Oster, grand masters of Mathematical Biology, to thank for the inspiration of the overall dynamical-systems and mechanochemical systems approach. More recently, single and collective cellular oscillations were accounted for by a generic oscillator model for turnover of force-producing material (such as myosin motors) contracting against an elastic element [46]. Similar to our results, varying the mechanical and kinetic properties of the

system can transition the cell behaviour from relaxed to oscillatory or contracted cell length and collective cell behaviour from unsynchronized to synchronized oscillations [46].

By coupling a simple GTPase bistable model (without spatially distributed activity within a cell) to a simple elastic (Kelvin–Voigt element) cell, we were able to show three distinct regimes of behavior, including high and low GTPase activity, with coordinated cell tension, and persistent periodic cycling between those states. Here the dynamic pattern of contractile activity stems exclusively from cell size fluctuations, amplified by tension-dependent GTPase activity. We did not include chemical diffusion (each cell is assumed to hold a uniform GTPase level), nor explicit cytoskeletal flows.

Actual signaling networks are of forbidding complexity, posing a significant challenge to our ability to understand how cell behavior emerges from underlying components and properties. Large networks have been studied theoretically, e.g. by [47–49]. For example, a detailed Boolean logic model of EGFR signaling in a cell with tens of nodes (CellNetAnalyzer) also showed cyclic/oscillatory activity of Rac1 and RhoA [47]. This level of detail is appropriate for asking specific questions about drug-targets in a real system. And yet, given this level of detail, understanding the connection between network features and parameters on one hand, and emergent cell behavior on the other, is challenging. First, the details of rates, interconnectivity, and even topology of the signaling networks are incompletely known. Second, even were we to simulate a topologically and quantitatively accurate copy of such networks, it would be very difficult to understand causal mechanisms due to combinatorial complexity. For this reason, stripped-down models that concentrate on key topologies and regulators have a role to play in the theoretical understanding of cell behavior [50]. This principle motivates our analysis of small models for the GTPases.

Assumptions we made for the purpose of simplification can be modified substantially without changing the overall conclusions. For example, while our equation for Rho activation resembles that of [15], their assumption about the Hill function-dependence on tension can be modified to another switch-like function that ‘turns on’ at some critical force magnitude. Furthermore, while there is so far evidence for the multiplicity of GEFs involved in mechanotransduction (relative to GAPs; see [17] table 1), our model works equally well with GAP-sensitive responses as with the GEF-based GTPase response assumed here.

One of our key findings here is that simple coupling between GTPase activity and tension is consistent with a range of biologically-relevant cell behavior. The simplest model already produces contracted or relaxed cells as well as cyclic fluctuations between these states. In the Rac-Rho circuit, such dynamic oscillatory regimes coexist with static steady states (in the same parameter range), highlighting the dependence on stimuli and/or initial conditions. Oscillations in

cell size are observed under laboratory conditions in epithelial monolayers [51, 52]. While the link between tension and GTPases may be just one factor operating in such systems, our model suggests experiments that could be used to test the connection. In particular, inhibitors of ROCK (that would abrogate the connection between RhoA and actomyosin contraction) or of Rac (that would inhibit the antagonism of Rac to Rho) could be used to test the effect on the presence, frequency, and synchrony of cell volume oscillations.

Hashimoto *et al* investigated the ‘zippering’ in the neural/epidermal boundary of the sea squirt (*Ciona intestinalis*) embryo, part of the process that sets up neurulation over a time frame of about 2 h [41]. Zippering involves successive shortening of cellular junctions, one after the other, in a unidirectional wave of contractions up the zippering axis. The contraction was shown to be powered by the localization of active myosin, along the boundary, and to be dependent on Rho/ROCK activity, based on its abrogation by blebbistatin and ROCK inhibitor (Y-27632) [41]. (Most dominant negative RhoA embryos failed to zipper.) The authors concluded that ‘local activation of actomyosin contractility by the RhoA/ROCK pathway at Ne/Epi junctions is required for junctional contraction, zippering, and neural tube closure’. Furthermore, their paper was accompanied by kinematic simulations that reproduced the sequence of contractions, based on assigned tensions (for pre- and post-contraction cells) and assigned time intervals.

Here we propose a simple model that aims at closing the gap between kinematics and dynamics. Briefly, we eschew the manual assignment of forces and time intervals, replacing these with a closed-loop chemical-mechanical system that can give rise to the wave-like pattern of sequential cell contractions. As shown in figure 5(D) and supplementary movie 4, under suitable conditions, a unidirectional wave of Rho activation and actomyosin contraction can be exhibited by our elementary model. The Hashimoto *et al* experiments support the presence of the basic elements (RhoA/ROCK activation and actomyosin contraction). That said, while our model could account for essential features of a wave of contraction seen in zippering, it is clear that other aspects (such as communication between cells reaching across the ‘zipper’ sides) play vital roles not considered here (Edwin Munro, personal communication).

In other organisms, such as *Drosophila*, Rac GTPase is known to have multiple roles in early morphogenesis [53]. During *Drosophila* dorsal closure, over- and under-expressing Rac results in the excess assembly of lamellipodia or disrupts the assembly of an actin cable (and subsequent zippering) and cell protrusions. While GTPases such as Rac regulate cell behavior during these morphogenetic processes, it is likely that cell and tissue mechanics also play an important role. Upstream mechanical signaling to Rho GTPases may occur as cells move and forces are transmitted, or

as cell–cell junctions are rearranged. In the case of zippering in sea squirt embryos, or in *Drosophila* dorsal closure, further validation of the mechanisms and/or completion of other essential elements remains as a future step. Nonetheless, with our mechanosensing assumptions, we have shown that feedback between signaling and mechanics can account for diverse single and collective cell behavior in these morphogenetic processes. Extending the conceptual model here to specific organisms by connecting to GTPase signaling and cell mechanics to data from experiments remains a direction for future work.

We focused on cell size (expanded or contracted), but it is also of interest to consider how cell polarization is affected by mechanical cues in isolated cells and in cell collectives. See [54] for some theoretical background and review. Importantly, our results point to parameter regimes in which cells oscillate between compression and relaxation (in the case of a single Rho-like GTPase), or compression and stretching (for Rac-Rho). But it is known that such cyclic stretching can itself change the properties of cells, reorganizing stress-fibers, for example in a Rho-dependent manner in endothelial cells [55]. It would be of interest to explore such polarity and directionality in future 2D models of this type, as well as to consider how the feedback between GTPases and tension operate in collective cell migration [56]. There is evidence that GTPases also affect the cell–cell adhesion [57, 58] and tight-junctions [59], which would affect the coupling of mechanical transduction between cells in a tissue. This could be of interest in future models.

Acknowledgments

We are very grateful to MoHan Zhang for his contribution to the project as an undergraduate summer research assistant (USRA) and to Jim Shaw for his contributions to the project as a volunteer undergraduate research assistant. We thank members of the Keshet-Feng research group for discussions and helpful suggestions. We are also grateful to Ajay Chitnis for discussions that sparked our interest in the link between cell collective behavior and GTPase dynamics. We are most grateful to the James Glazier group for making CompuCell3D publicly available. We acknowledge the support of the Natural Sciences and Engineering Research Council of Canada (NSERC) [Discovery Grant 41870 to LEK].

Competing interests

The authors declare that they have no competing interests.

Appendix. Numerical methods

Numerical integration of the single cell models and bifurcation analysis was preformed using PyDSTool

[60]. Numerical integration of the single cell and multicellular models was preformed using MATLAB 2017a (The MathWorks, Inc. Natick, Massachusetts, United States). Cellular Potts model simulations were produced with CompuCell3D [42].

A.1. Scaling the GTPase model

The dynamics of active GTPase are governed by the following differential equation:

$$\frac{dG}{dt} = \left(\hat{b} + \hat{\gamma} \frac{G^n}{G_0^n + G^n} \right) (G_T - G) - \delta G. \quad (\text{A.1})$$

Here, \hat{b} is a basal activation rate, $\hat{\gamma}$ gives the magnitude of the positive feedback upon the activation rate, and G_0 describes the concentration of GTPase at which positive feedback reaches its half-maximal effect. $G_T - G$ gives the total concentration of inactive GTPase.

To reduce the size of parameter space, we scale GTPase concentration by the half-max quantity G_0 , and we scale time by the active GTPase residence time $1/\delta$, respectively. The equations become

$$\frac{dG}{dt} = \left(b + \gamma \frac{G^n}{1 + G^n} \right) (G_T - G) - G. \quad (\text{A.2})$$

The mechanical stimulus term $f(T)$ was added to the activation rate, i.e. we assumed that it operates via a GEF. We considered several forms of mechanical feedback from cell deformation to GTPase activity. Based on the idea that the difference between the current cell ‘length’ L and the current cell ‘rest-length’ L_0 creates the tension that stimulates mechanosensitive pathways, we can express that feedback in terms of L and L_0 . Consequently, we experimented with each of the following forms:

$$\begin{aligned} f_0(L) &= \beta(L - L_0), && \text{Linear case;} \\ f_1(L) &= \beta \frac{L^m}{L_0^m + L^m}, && \text{Hill function;} \\ f_2(L) &= \beta \frac{1}{1 + \exp[\alpha(L - L_0)]}, && \text{Squashing function;} \\ f_3(L) &= \beta \frac{1}{1 + \exp\left[\alpha \frac{(L - L_0)}{L_0}\right]}, && \text{Strain-dependent squashing function.} \end{aligned}$$

All four cases share the property that GTPase activation is amplified if $L \gg L_0$. The linear function f_0 has the property that both stretching ($L > L_0$) and compression ($L < L_0$) affect GTPase activation, albeit in opposite ways (stretching increases while compression decreases the GTPase activation rate.) The squashing function f_2 is predominately unidirectional, i.e. only $L > L_0$ has a significant effect, so stretching, but not compressing a cell affects its signaling. This function was used in our minimal model and has the advantage of specifically tracking tension. At the same time, f_1 has a similar effect as f_2 , and was to a large extent indistinguishable in the dynamical results we obtained (see figure A1(B) for a bifurcation diagram of the single-cell model with the Hill function response f_1). The noticeable difference occurs in the synchronization of large tissue simulations. Compare, for example, the simulation with the squashing function f_2 in figure 5(E) and

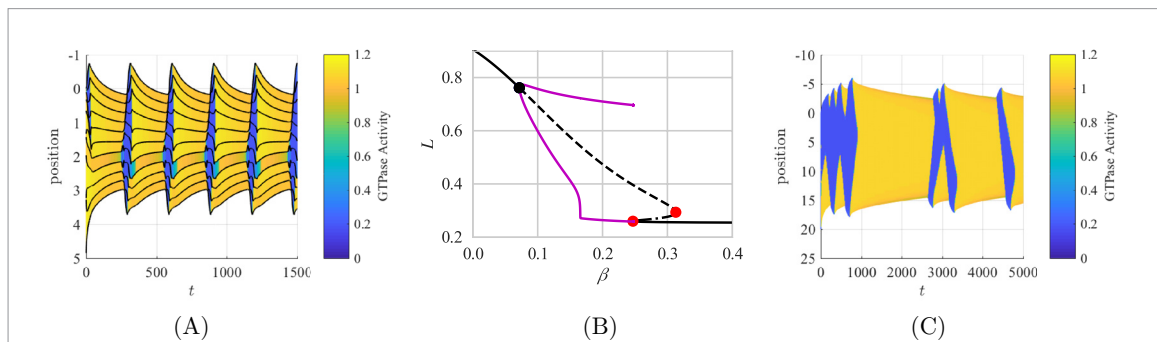


Figure A1. Additional 1D tissue dynamics result from mechanochemical interactions. Kymographs show the 1D position of each cell (vertical axis) with color indicating the GTPase activity within each cell. In (A), a single oscillatory cell with $\beta = 0.2$ can induce tissue-level oscillations among a population of contracted cells with $\beta = 0.3$. In (B), single cell dynamics with the Hill function response from tension, $f_1(T)$, qualitatively resemble the dynamics with the squashing function $f_2(T)$. In (C), waves of contraction propagate through the tissue of 50 oscillatory cells ($\beta = 0.2$) with the strain-dependent feedback, $f_3(T)$. See also supplementary movies 10 and 11, for (A) and (C) respectively.

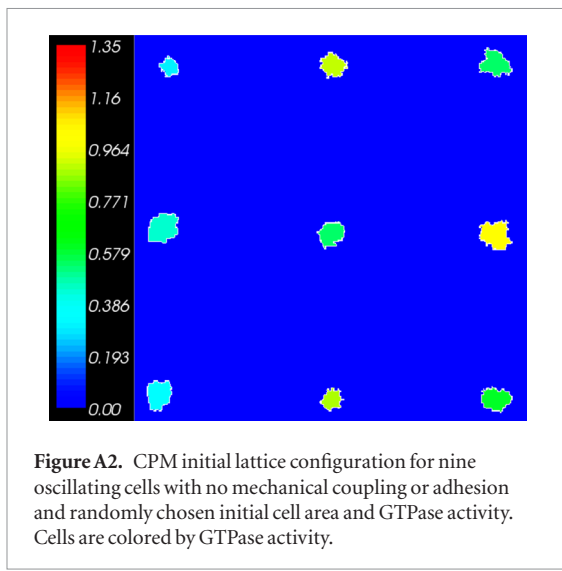


Figure A2. CPM initial lattice configuration for nine oscillating cells with no mechanical coupling or adhesion and randomly chosen initial cell area and GTPase activity. Cells are colored by GTPase activity.

the simulation with the strain-dependent squashing function f_3 in figure A1(C).

The Hill function and strain-dependent squashing function, f_1 and f_3 have a similar shape for all L and L_0 and are approximately equal for the parameters used herein. The change that f_1 and f_3 can affect in the GTPase activation rate is relative to the current rest-length of the cell L_0 . This is different from the squashing function f_2 , which assumes a mechanosensing mechanism by which tension can activate GTPase signaling regardless of the current rest length, L_0 .

The Rac-Rho mutual inhibition model in section 5 equation (5.1), is the scaled model. Details of this scaling are similar to scaling for the single GTPase model. The reader is referred to [29, 39].

A.2. 1D methods: multicellular simulations

Equations (3.1) and (2.2a) were implemented in a collection of cells in 1D. Each cell has its own GTPase activity G_j , which is described by equation (2.2a), with lengths given by $L_j = x_{n+1} - x_j$. Numerical integration was done using MATLAB 2017a (The MathWorks,

Inc. Natick, Massachusetts, United States) for all 1D multicellular simulations.

For figures 5(A)–(C), (E), and (F), and A1(A) and (B), GTPase activity in each cell, G_j , affects the rest length through

$$L_{j,0} = \ell_0 - \phi \frac{G_j^p}{G_h^p + G_j^p}. \quad (\text{A.3})$$

Tension is assumed to affect the GTPase activation rate through the squashing function response to tension (f_2 above, also equation (2.2b)). Parameter values for these simulations are $b = 0.1$, $\gamma = 1.5$, $n = p = 4$, $G_T = 2$, $\alpha = 10$, $\ell_0 = 1$, $\phi = 0.75$, $G_h = 0.3$, $k = 1$, $\lambda = 10$, and β varies. Initial conditions are $L_j(0) = 0.7$ and $G_j(0) = 1$ for the $N = 10$ simulations, and random initial lengths with $G_j(0) = 1$ for all simulations with $N > 10$ and for the $N = 10$ case with one oscillatory cell, figure A1. Instead of the squashing function response to tension (f_2), the strain-dependent squashing function (f_3) was used in figure A1(c).

For figure 5(D), we simulated $N = 14$ cells, and assumed linear responses for both GTPase-activation from tension (f_0) and for rest-length from GTPase activity:

$$L_{j,0} = \ell_0 - \phi G_j. \quad (\text{A.4})$$

Initial conditions for this simulation were $L_j(0) = 0.68$, $n = 1, \dots, 14$, $G_j(0) = 0.45$ for all j with the exception of, and $G_j(0) = 1.2$ for $j = 13, 14$. Other parameters were $b = 0.3$, $\beta = 0.35$, $\ell_0 = 1$, $\phi = 0.7$, $n = 4$, $G_T = 1.75$, $k = 1$, and $\lambda = 10$.

A.3. 2D methods: cellular Potts model

We use CompuCell3D, an open-source implementation of the cellular Potts model, for 2D simulations of the GTPase-tension model [42]. The cellular Potts model is an individual cell-based model where each cell occupies one or more discrete lattice sites. Cells can expand outwards or contract inwards by adding or removing lattice sites at the cell perimeter. The dynamics of each

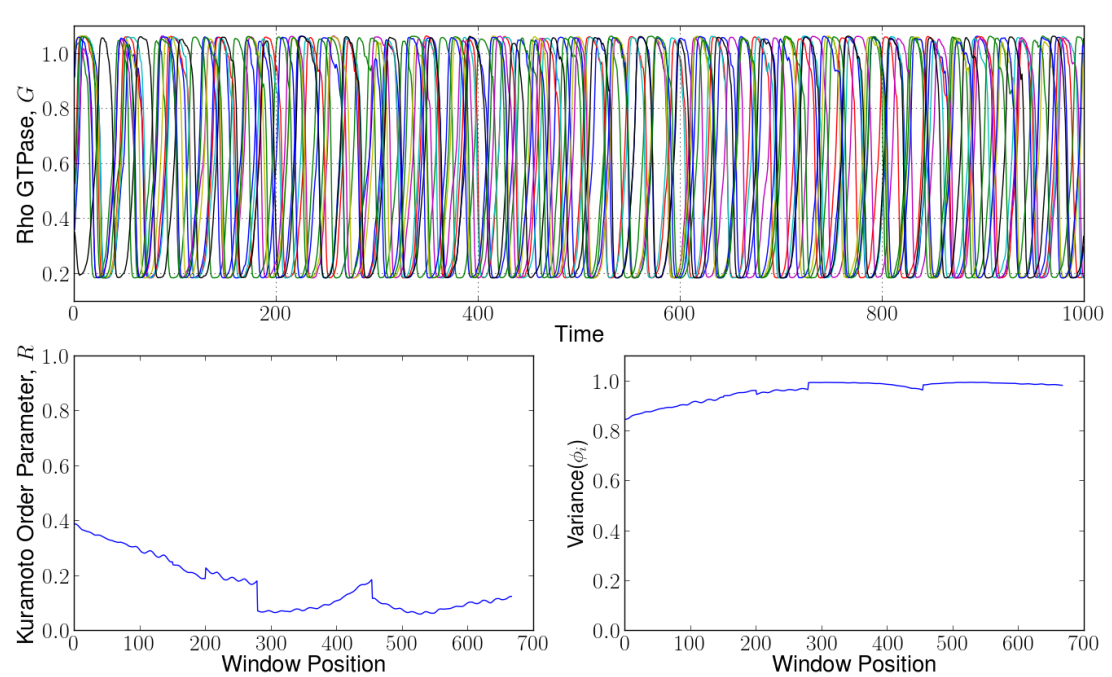


Figure A3. Time series of GTPase activity, Kuramoto order parameter and variance in phase for nine independent oscillators shown figure A2. Note that initial cell area is equal to initial cell target area, hence initial conditions are not fully randomized. Variance increases with time due to the stochastic nature of spin copy attempts that offset the initial conditions.

‘cell’ is governed by a Hamiltonian energy function, \mathcal{H} . The Hamiltonian for our 2D simulation consists of an area constraint term (also called volume deformation term in a general 3D context) and an adhesion energy term. The area constraint is implemented in terms of a (time-varying) target area. Target area represents the area (number of lattice sites) that each cell would occupy in an optimal lattice configuration. The adhesion energies specify the interactions between different cells and the surrounding medium (extra-cellular space, or ‘medium’). Additionally, a connectivity constraint is imposed that penalizes the Hamiltonian if lattice sites for each cell do not form a connected domain. This avoids fragmentation of the ‘cells’.

Lattice sites are added or removed from cells in ‘spin-copy attempts’. A spin-copy attempt is accepted if it decreases the overall energy of the system, as defined by the Hamiltonian. A spin-copy attempt is also accepted with a non-zero probability if it results in a small increase in the Hamiltonian. The temperature parameter in the Boltzmann distribution of accepted unfavourable spin-copies controls the degree of exploration of energetically unfavourable lattice configurations. Given N lattice sites, a collection of N spin-copy attempts constitutes one Monte-Carlo step (MCS) of the simulation. The Metropolis algorithm is used to determine the quasi-deterministic kinetics of lattice configurations evolving under the Hamiltonian. While CPM does not explicitly track forces, it has recently been shown to correspond to other vertex-based simulations where forces are made explicit [43].

The target area for a cell is determined by a system of ODEs that couple sub-cellular biochemistry (assuming that the cell is well-mixed) to cell mechanics. To adapt the model to the technical requirements of the CPM,

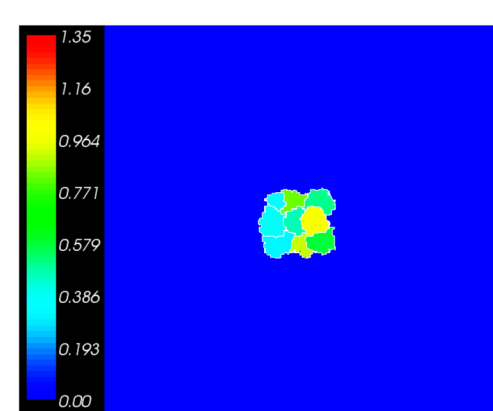


Figure A4. CPM initial lattice configuration for nine oscillating mechanically coupled cells with randomly chosen initial cell area and GTPase activity. Each lattice site can only be occupied by one cell and overlap is not allowed. Cell-cell and cell-medium adhesion parameters govern the mechanical interactions of the cells. Strength of adhesion between cells is higher if cell-cell adhesion energy is lower compared to cell-medium adhesion energy, and vice-versa. Cells are colored by GTPase activity.

we had to select an appropriate timescale. We also had to create a dynamical equation for the target area.

$$\frac{1}{\tau} \frac{dG}{dt} = \left(b + f(T) + \gamma \frac{G^n}{1 + G^n} \right) (G_T - G) - G, \quad (\text{A.5a})$$

$$\frac{1}{\tau} \frac{dA_T}{dt} = -\varepsilon(A_T - A_0(G)), \quad \text{where} \\ A_0(G) = a_0 \left(1 - \phi \frac{G^p}{G_h^p + G^p} \right). \quad (\text{A.5b})$$

a_0 is the constant baseline cell area. The target area A_T approaches A_0 on the timescale τ that we can control

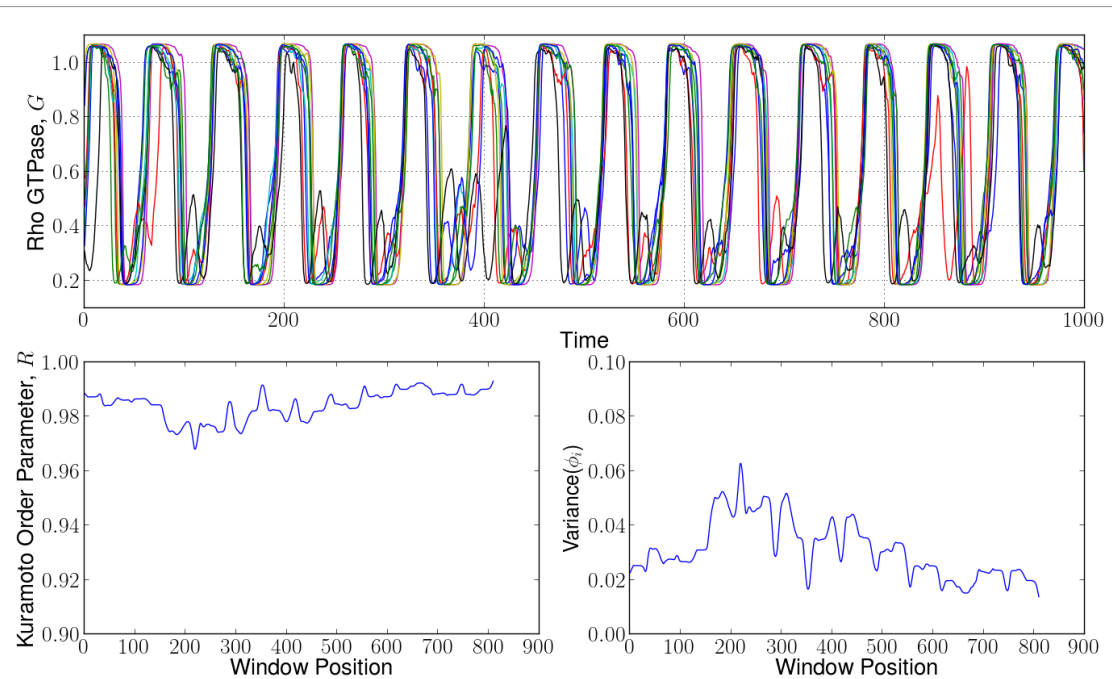


Figure A5. Synchronized oscillations in the low adhesion regime in a simulation as in figure A4 over 1000 MCS. Cell–medium adhesion energy (40) is less than cell–cell adhesion energy (80) in the Hamiltonian \mathcal{H} . Adhesion strength is low, which implies less entrainment/synchrony.

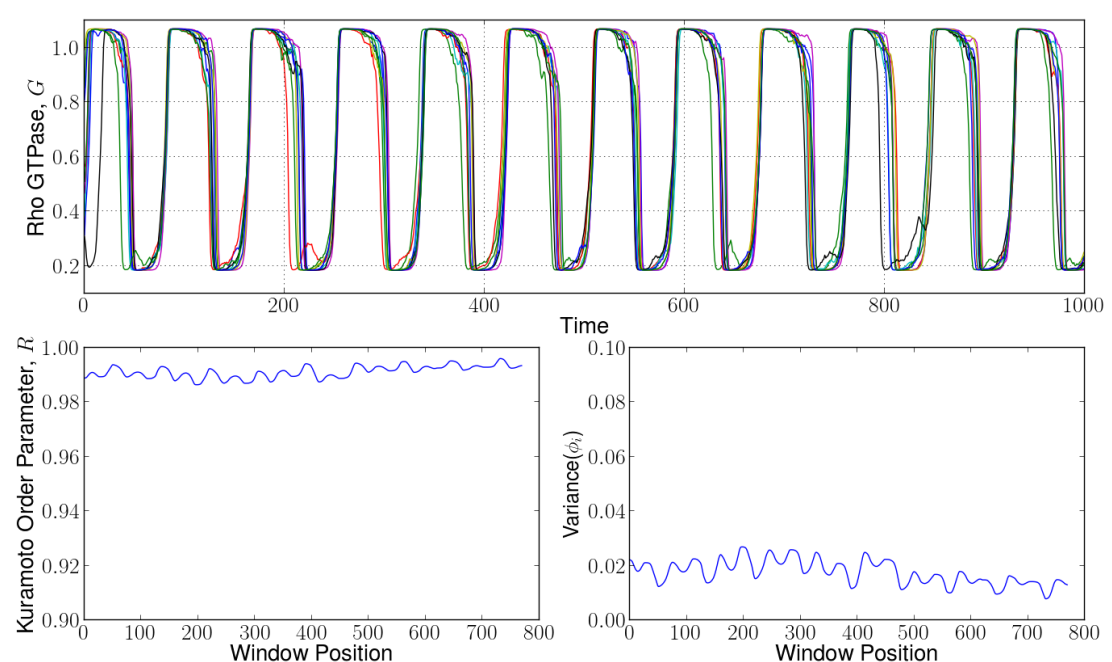


Figure A6. Synchronization in the intermediate adhesion regime. Cell–medium adhesion energy (80) is equal to cell–cell adhesion energy (80) in the Hamiltonian \mathcal{H} .

to increase or decrease the speed of the feedback. Note that cell area (A) does not approach target area (A_T) instantaneously, but through the addition or removal of lattice sites over several MCS. That is, A , is updated stochastically to approach the target area A_T by the CPM.

We also assumed

$$f(T) = \beta \frac{A^m}{A_T^m + A^m}, \quad \text{where} \quad T = A - A_T. \quad (\text{A.5c})$$

Here the tension is defined as $T = (A - A_T)$, which is a ‘delayed’ form of $(A - A_0)$. In turn, the function $f(T)$, describes the feedback on GTPase activation from tension. This Hill function has the property that as m increases, its shape is fundamentally similar to that of the squashing function used in the 1D GTPase model in the main paper equation (2.2b). For this initial exploration, we assumed that GTPase activity was uniform inside a given cell (through variable across the entire collection of cells). This dramatically decreases

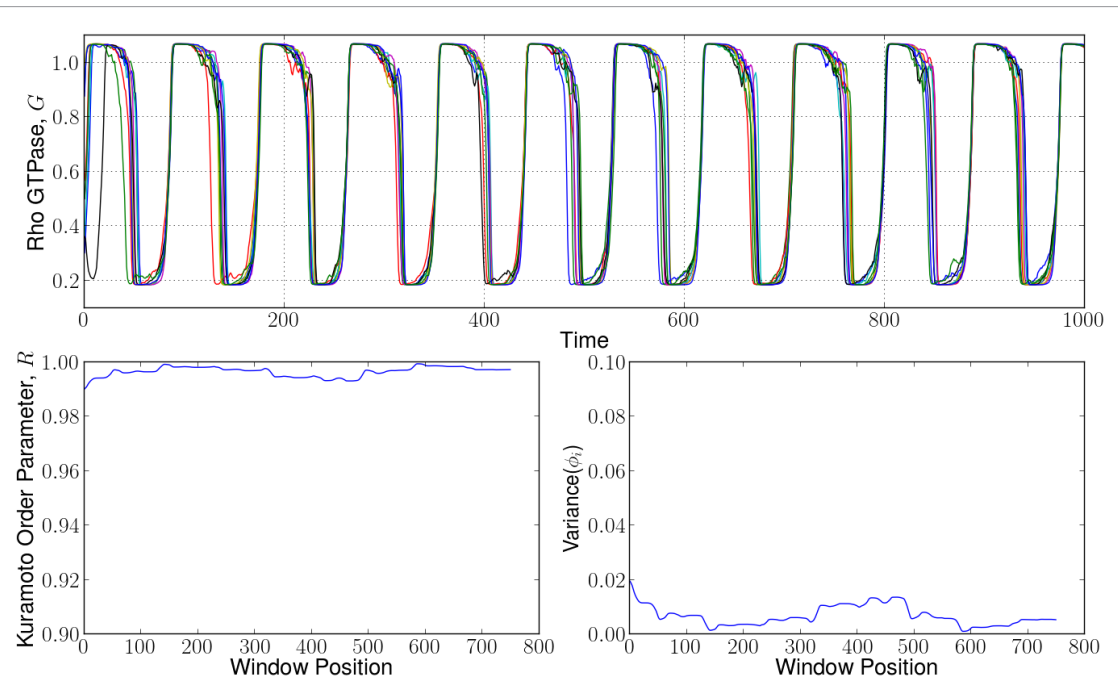


Figure A7. Synchronization in the high adhesion regime. Cell–cell adhesion energy (60) is less than cell–medium adhesion energy (80) in the Hamiltonian \mathcal{H} . This implies high degree of adhesion strength between cells, leading to entrainment.

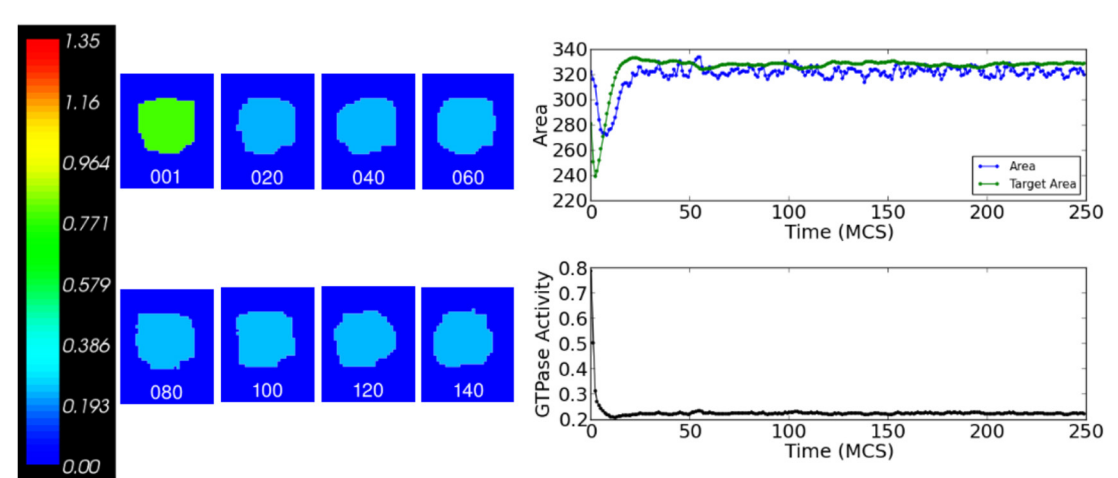


Figure A8. Relaxed cell with low Rho GTPase activity, $\beta = 0.05$. Cells are colored by GTPase activity. Cell area, target area, and GTPase activity are plotted over time.

the complexity of the simulation. Stochasticity in the CPM leads to interesting behavior (e.g. stochastic switching) which is not observed in deterministic numerical solutions.

As before, we have assumed that increasing tension (represented as the difference between target area and actual cell area), can increase GTPase activity via equation (A.5c). To appropriately calibrate the model to observe the same oscillatory dynamics as in the one-cell single GTPase model, we chose the time-scale and the time step for numerically integrating the ODEs, τ and Δt , respectively, so that each MCS is $\tau \Delta t = 2000 \cdot 0.001 = 2$ units of time t .

In the case of single cells, the model parameters are $\tau = 2000$, $b = 0.1$, $m = 10$, $\gamma = 1.5$, $n = p = 4$, $G_T = 2$, $\varepsilon = 0.1$, $a_0 = 400$, $\phi = 0.75$, and $G_h = 0.3$. Sin-

gle cell simulations ran for 250 MCS, with temperature parameter 30. The cell–cell and cell–medium adhesion energies are set to 0.1 and 80 in the Hamiltonian \mathcal{H} , respectively, and we did not impose a perimeter (surface) constraint. The area constraint parameter in the Hamiltonian \mathcal{H} was set to $\lambda_A = 1$ and initial conditions were set as $G(0) = 1$, $A_T(0) = 320$, and $A(0) = 320$.

A.4. 2D methods: patch size and synchronization

To explore the idea that adhesion strength could affect the extent of synchrony among the cells in the tissue, we varied the adhesion energy in the Hamiltonian \mathcal{H} among a small tissue of nine cells, with each cell in the oscillatory regime. We treated the tissue as a system of coupled oscillators and numerically quantified the level of synchrony using the Kuramoto order

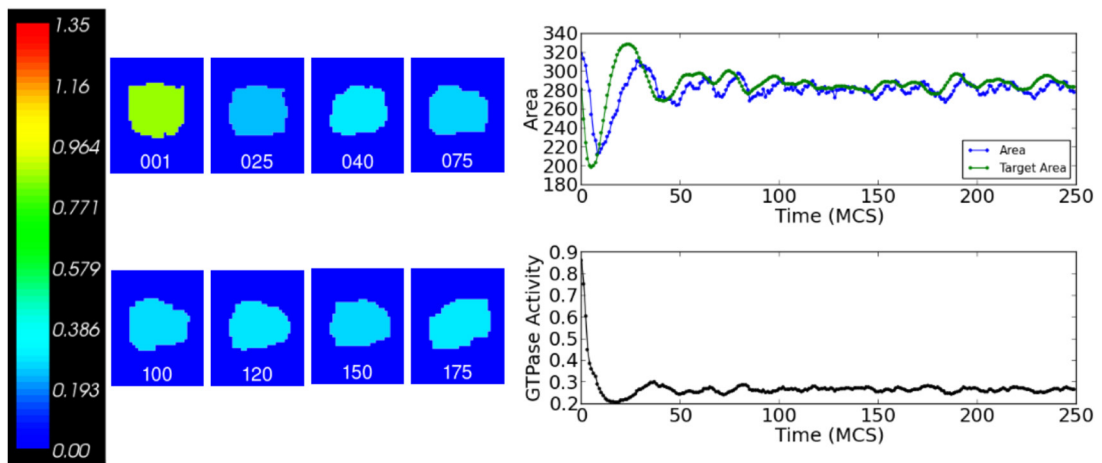


Figure A9. Damped oscillations for $\beta = 0.1$. Cells are colored by GTPase activity. Cell area, target area, and GTPase activity are plotted over time.

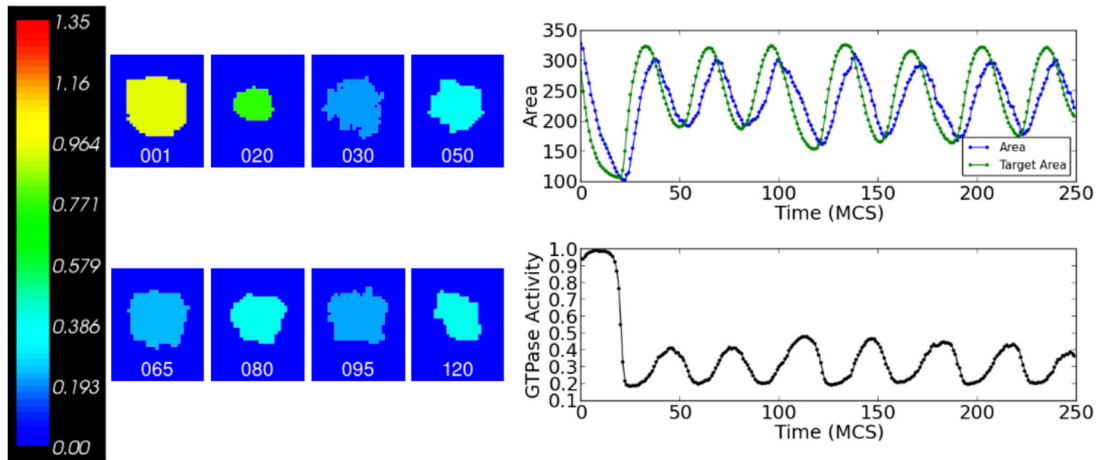


Figure A10. Small amplitude limit cycle, $\beta = 0.15$. Cells are colored by GTPase activity. Cell area, target area, and GTPase activity are plotted over time.

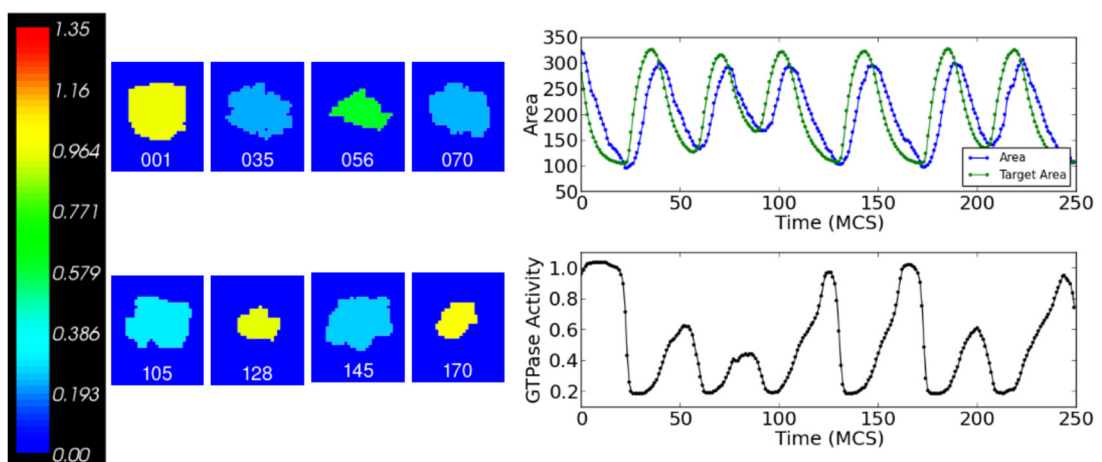


Figure A11. Stochastic switching between low amplitude limit cycle and high amplitude limit cycle, $\beta = 0.175$. Cells are colored by GTPase activity. Cell area, target area, and GTPase activity are plotted over time.

parameter and the variance in the distribution of phase angles of the oscillators. The Kuramoto order parameter describes the degree of synchronization in

a collection of coupled oscillators (see [61], or [62] for a review). As adhesion-strength increases, we find that the oscillators are more synchronized, with an

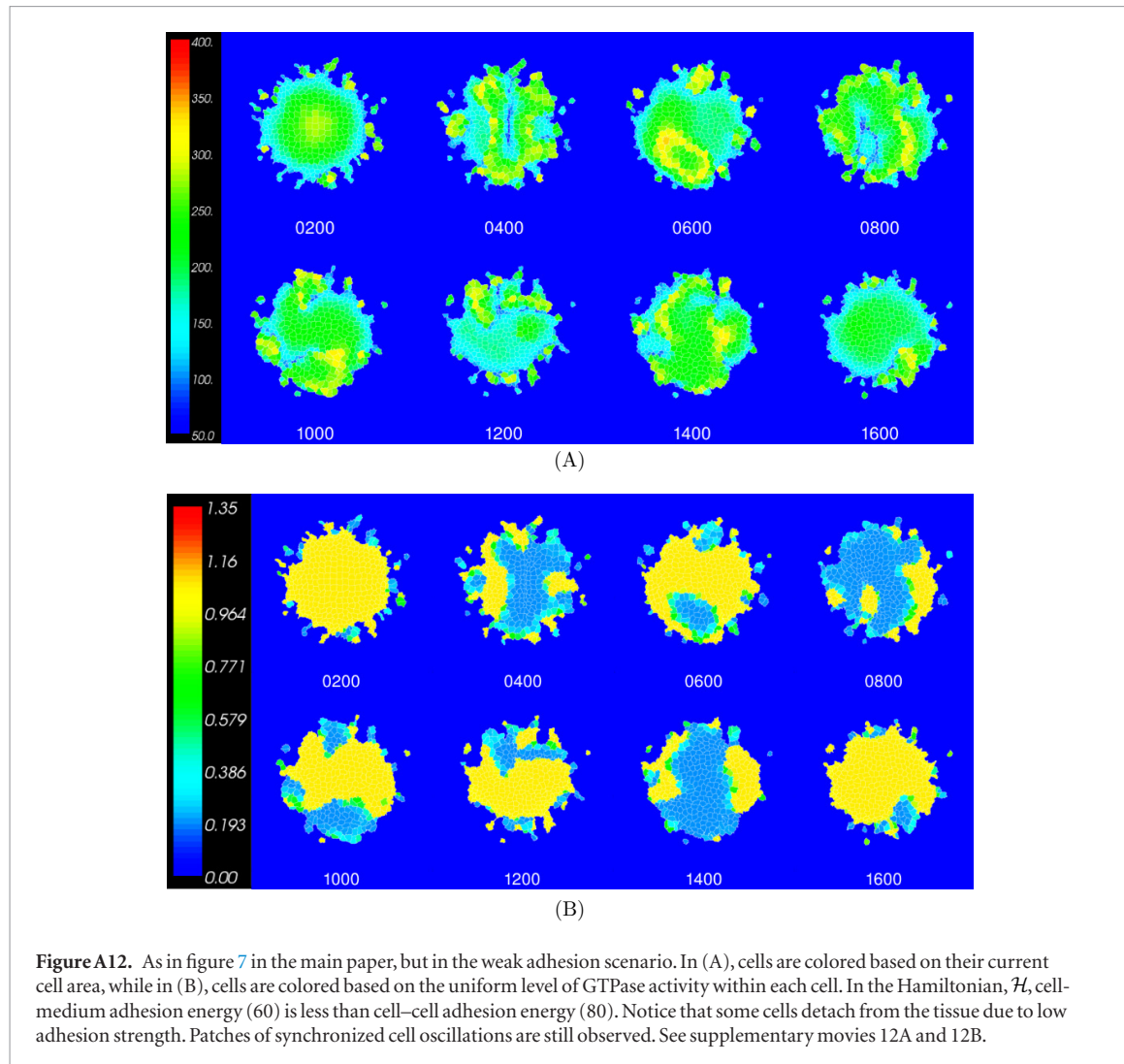


Figure A12. As in figure 7 in the main paper, but in the weak adhesion scenario. In (A), cells are colored based on their current cell area, while in (B), cells are colored based on the uniform level of GTPase activity within each cell. In the Hamiltonian, \mathcal{H} , cell-medium adhesion energy (60) is less than cell-cell adhesion energy (80). Notice that some cells detach from the tissue due to low adhesion strength. Patches of synchronized cell oscillations are still observed. See supplementary movies 12A and 12B.

apparent increase in the Kuramoto order parameter, and a decrease in variance in the distribution of phase angles. See figures A3 and A5–A7.

To determine the Kuramoto order parameter for the small tissue, the dominant frequency of each oscillating cell (i.e. frequency with highest magnitude) is determined over time using a sliding window with the real-valued Fourier transform (RFFT). The fixed size window contains time series data roughly equivalent to 3 periods of oscillation. The Kuramoto order parameter and variance in phase is calculated by determining the phase corresponding to the dominant frequency for all nine oscillators.

Model parameters are as in appendix A.3, except the initial conditions for cell areas are randomly chosen, initial conditions for GTPase are randomly chosen between 0 and 1 and initial target area is also randomly chosen between 350 and 450.

A.5. 2D methods: large-tissue simulations

A circular tissue consisting of 373 cells with randomly chosen area (and $\beta = 0.2$, corresponding to the oscillatory regime) is used as the initial lattice configuration. Initial target area was set to the initial cell area for each cell (between 300 to 400 lattice sites). The simulation was

carried out for 2000 MCS. Initial GTPase concentration is randomly chosen between 0 and 1. The remaining model parameters are as in appendix A.3.

A.6. Additional 2D results

In this section, some additional 2D CPM simulation results are presented. Model parameters are as before, outlined in appendix A.3. Each figure shows 8 snapshots of the cell behavior, with the color indicating the GTPase activity. Also shown are the cell area, target area, and the GTPase activity over time. These results include:

- (1) Figure A8: a single relaxed cell with large constant area and low GTPase activity with $\beta = 0.05$.
- (2) Figure A9: damped oscillations occur for $\beta = 0.1$.
- (3) Figure A10: a small amplitude limit cycle with $\beta = 0.15$.
- (4) Figure A11: stochastic switching between a low amplitude limit cycle and high amplitude limit cycle with $\beta = 0.175$.

Also, a large tissue simulation similar to figures 7 and 8 but with weak adhesion is shown in figure A12.

A.7. The Rac-Rho model

In our Rac-Rho model, we used the following system of equations:

$$\frac{dR}{dt} = \frac{b_R}{1 + \rho^n} (R_T - R) - \delta R, \quad (\text{A.6a})$$

$$\frac{d\rho}{dt} = (b_\rho + f(T)) \frac{1}{1 + R^n} (\rho_T - \rho) - \rho, \quad (\text{A.6b})$$

where $f(T)$ models the activation of Rho GTPase by tension:

$$f(T) = \gamma_\rho \frac{1}{1 + \exp[-\alpha(L - L_0)]}, \quad \text{where } T = L - L_0. \quad (\text{A.6c})$$

As before, Rho GTPase activity decreases the rest-length of the cell:

$$\frac{dL}{dt} = -\varepsilon (L - L_0), \quad \text{where } L_0 = \ell_0 - \phi \frac{\rho^p}{\rho_h^p + \rho^p}. \quad (\text{A.6d})$$

ORCID iDs

- Cole Zmurchok  <https://orcid.org/0000-0003-2368-5658>
 Dhananjay Bhaskar  <https://orcid.org/0000-0001-8068-3101>
 Leah Edelstein-Keshet  <http://orcid.org/0000-0002-2233-690X>

References

- [1] Ridley AJ 2001 Rho family proteins: coordinating cell responses *Trends Cell Biol.* **11** 471–7
- [2] Van Keymeulen A, Wong K, Knight ZA, Govaerts C, Hahn K M, Shokat K M and Bourne H R 2006 To stabilize neutrophil polarity, PIP3 and Cdc42 augment RhoA activity at the back as well as signals at the front *J. Cell Biol.* **174** 437–45
- [3] Wong K, Pertz O, Hahn K and Bourne H 2006 Neutrophil polarization: spatiotemporal dynamics of RhoA activity support a self-organizing mechanism *Proc. Natl Acad. Sci. USA* **103** 3639–44
- [4] Otsuji M, Ishihara S, Co C, Kaibuchi K, Mochizuki A and Kuroda S 2007 A mass conserved reaction–diffusion system captures properties of cell polarity *PLoS Comput. Biol.* **3** e108
- [5] Mori Y, Jilkine A and Edelstein-Keshet L 2008 Wave-pinning and cell polarity from a bistable reaction-diffusion system *Biophys. J.* **94** 3684–97
- [6] Nobes CD and Hall A 1999 Rho GTPases control polarity, protrusion, and adhesion during cell movement *J. Cell Biol.* **144** 1235–44
- [7] Fukata M, Nakagawa M and Kaibuchi K 2003 Roles of Rho-family GTPases in cell polarisation and directional migration *Curr. Opin. Cell Biol.* **15** 590–7
- [8] Ridley AJ 2015 Rho GTPase signalling in cell migration *Curr. Opin. Cell Biol.* **36** 103–12
- [9] Discher D E, Janmey P and Wang Y-L 2005 Tissue cells feel and respond to the stiffness of their substrate *Science* **310** 1139–43
- [10] Vogel V and Sheetz M 2006 Local force and geometry sensing regulate cell functions *Nat. Rev. Mol. Cell Biol.* **7** 265–75
- [11] Sabass B, Gardel M L, Waterman C M and Schwarz U S 2008 High resolution traction force microscopy based on experimental and computational advances *Biophys. J.* **94** 207–20
- [12] Diz-Muñoz A, Fletcher D A and Weiner O D 2013 Use the force: membrane tension as an organizer of cell shape and motility *Trends Cell Biol.* **23** 47–53
- [13] Pertz O and Hahn K M 2004 Designing biosensors for Rho family proteins—deciphering the dynamics of Rho family GTPase activation in living cells *J. Cell Sci.* **117** 1313–8
- [14] Houk A R, Jilkine A, Mejean C O, Boltynski I, Dufresne E R, Angenent S B, Altschuler S J, Wu L F and Weiner O D 2012 Membrane tension maintains cell polarity by confining signals to the leading edge during neutrophil migration *Cell* **148** 175–88
- [15] He L, Tao J, Maity D, Si F, Wu Y, Wu T, Prasath V, Wirtz D and Sun S X 2018 Role of membrane-tension gated Ca²⁺ flux in cell mechanosensation *J. Cell Sci.* **131** jcs208470
- [16] Katsumi A, Milanini J, Kiosses W B, Del Pozo M A, Kaunas R, Chien S, Hahn K M and Schwartz M A 2002 Effects of cell tension on the small GTPase Rac *J. Cell Biol.* **158** 153–64
- [17] Ohashi K, Fujiwara S and Mizuno K 2017 Roles of the cytoskeleton, cell adhesion and rho signalling in mechanosensing and mechanotransduction *J. Biochem.* **161** 245–54
- [18] Freeman S A, Christian S, Austin P, Iu I, Graves M L, Huang L, Tang S, Coombs D, Gold M R and Roskelley C D 2017 Applied stretch initiates directional invasion through the action of Rap1 GTPase as a tension sensor *J. Cell Sci.* **130** 152–63
- [19] Pines M, Das R, Ellis S J, Morin A, Czerniecki S, Yuan L, Klose M, Coombs D and Tanentzapf G 2012 Mechanical force regulates integrin turnover in *Drosophila* *in vivo* *Nat. Cell Biol.* **14** 935–43
- [20] Kumar A, Ouyang M, Van den Dries K, McGhee E J, Tanaka K, Anderson M D, Groisman A, Goult B T, Anderson K I and Schwartz M A 2016 Talin tension sensor reveals novel features of focal adhesion force transmission and mechanosensitivity *J. Cell Biol.* **213** 371–83
- [21] Diz-Muñoz A, Thurley K, Chintaman S, Altschuler S J, Wu L F, Fletcher D A and Weiner O D 2016 Membrane tension acts through PLD2 and mTORC2 to limit actin network assembly during neutrophil migration *PLoS Biol.* **14** e1002474
- [22] Das T, Safferling K, Rausch S, Grabe N, Boehm H and Spatz J P 2015 A molecular mechanotransduction pathway regulates collective migration of epithelial cells *Nat. Cell Biol.* **17** 276–87
- [23] Tomar A and Schlaepfer D D 2009 Focal adhesion kinase: switching between GAPs and GEFs in the regulation of cell motility *Curr. Opin. Cell Biol.* **21** 676–83
- [24] Tsujita K, Takenawa T and Itoh T 2015 Feedback regulation between plasma membrane tension and membrane-bending proteins organizes cell polarity during leading edge formation *Nat. Cell Biol.* **17** 749–58
- [25] Odell G, Oster G, Burnside B and Alberch P 1980 A mechanical model for epithelial morphogenesis *J. Math. Biol.* **9** 291–5
- [26] Odell G M, Oster G, Alberch P and Burnside B 1981 The mechanical basis of morphogenesis: I. epithelial folding and invagination *Dev. Biol.* **85** 446–62
- [27] Oster G F, Murray J D and Harris A K 1983 Mechanical aspects of mesenchymal morphogenesis *Development* **78** 83–125 (PMID: 6663234)
- [28] Park J, Holmes W R, Lee S H, Kim H-N, Kim D-H, Kwak M K, Wang C J, Edelstein-Keshet L and Levchenko A 2017 Mechanochemical feedback underlies coexistence of qualitatively distinct cell polarity patterns within diverse cell populations *Proc. Natl Acad. Sci. USA* **114** E5750–9
- [29] Holmes W R, Park J, Levchenko A and Edelstein-Keshet L 2017 A mathematical model coupling polarity signaling to cell adhesion explains diverse cell migration patterns *PLoS Comput. Biol.* **13** e1005524
- [30] Bakal C, Aach J, Church G and Perrimon N 2007 Quantitative morphological signatures define local signaling networks regulating cell morphology *Science* **316** 1753–6
- [31] Sailem H, Bousgouni V, Cooper S and Bakal C 2014 Cross-talk between Rho and Rac GTPases drives deterministic exploration of cellular shape space and morphological heterogeneity *Open Biol.* **4** 130132
- [32] Cooper S, Sadok A, Bousgouni V and Bakal C 2015 Apolar and polar transitions drive the conversion between amoeboid and mesenchymal shapes in melanoma cells *Mol. Biol. Cell* **26** 4163–70

- [33] Byrne K M *et al* 2016 Bistability in the Rac1, PAK, and RhoA signaling network drives actin cytoskeleton dynamics and cell motility switches *Cell Syst.* **2** 38–48
- [34] Rottner K, Hall A and Small J 1999 Interplay between Rac and Rho in the control of substrate contact dynamics *Curr. Biol.* **9** 640–8
- [35] Machacek M, Hodgson L, Welch C, Elliott H, Pertz O, Nalbant P, Abell A, Johnson G, Hahn K and Danuser G 2009 Coordination of Rho GTPase activities during cell protrusion *Nature* **461** 99–103
- [36] Guilluy C, Garcia-Mata R and Burridge K 2011 Rho protein crosstalk: another social network? *Trends Cell Biol.* **21** 718–26
- [37] Parri M and Chiarugi P 2010 Rac and Rho GTPases in cancer cell motility control *Cell Commun. Signal.* **8** 23
- [38] Marée A F, Jilkine A, Dawes A, Grieneisen V A and Edelstein-Keshet L 2006 Polarization and movement of keratocytes: a multiscale modelling approach *Bull. Math. Biol.* **68** 1169–211
- [39] Holmes W R and Edelstein-Keshet L 2016 Analysis of a minimal Rho-GTPase circuit regulating cell shape *Phys. Biol.* **13** 046001
- [40] Jilkine A, Marée A F and Edelstein-Keshet L 2007 Mathematical model for spatial segregation of the Rho-family GTPases based on inhibitory crosstalk *Bull. Math. Biol.* **69** 1943–78
- [41] Hashimoto H, Robin F B, Sherrard K M and Munro E M 2015 Sequential contraction and exchange of apical junctions drives zippering and neural tube closure in a simple chordate *Dev. Cell* **32** 241–55
- [42] Swat M H, Thomas G L, Belmonte J M, Shirinifard A, Hmeliak D and Glazier J A 2012 *Multi-Scale Modeling of Tissues Using CompuCell3D (Methods in Cell Biology)* ed A R Asthagiri and A P Arkin (New York: Academic) pp 325–66
- [43] Magno R, Grieneisen V A and Marée A F 2015 The biophysical nature of cells: potential cell behaviours revealed by analytical and computational studies of cell surface mechanics *BMC Biophys.* **8** 8
- [44] Gross P, Kumar K V and Grill S W 2017 How active mechanics and regulatory biochemistry combine to form patterns in development *Annu. Rev. Biophys.* **46** 337–56
- [45] Wang W, Tao K, Wang J, Yang G, Ouyang Q, Wang Y, Zhang L and Liu F 2017 Exploring the inhibitory effect of membrane tension on cell polarization *PLoS Comput. Biol.* **13** e1005354
- [46] Dierkes K, Sumi A, Solon J and Salbreux G 2014 Spontaneous oscillations of elastic contractile materials with turnover *Phys. Rev. Lett.* **113** 148102
- [47] Hetmanski J H, Zindy E, Schwartz J-M and Caswell P T 2016 A MAPK-driven feedback loop suppresses Rac activity to promote RhoA-driven cancer cell invasion *PLoS Comput. Biol.* **12** e1004909
- [48] Kim T-H, Monsefi N, Song J-H, von Kriegsheim A, Vandamme D, Pertz O, Kholodenko B N, Kolch W and Cho K-H 2015 Network-based identification of feedback modules that control RhoA activity and cell migration *J. Mol. Cell Biol.* **7** 242–52
- [49] Marée A F M, Grieneisen V A and Edelstein-Keshet L 2012 How cells integrate complex stimuli: The effect of feedback from phosphoinositides and cell shape on cell polarization and motility *PLoS Comput. Biol.* **8** e1002402
- [50] Tsyanov M A, Kolch W and Kholodenko B N 2012 The topology design principles that determine the spatiotemporal dynamics of G-protein cascades *Mol. BioSyst.* **8** 730–43
- [51] Zehnder S M, Stuaris M, Bellaire M M and Angelini T E 2015 Cell volume fluctuations in MDCK monolayers *Biophys. J.* **108** 247–50
- [52] Zehnder S M, Wiatt M K, Uruena J M, Dunn A C, Sawyer W G and Angelini T E 2015 Multicellular density fluctuations in epithelial monolayers *Phys. Rev. E* **92** 032729
- [53] Woolner S, Jacinto A and Martin P 2005 The small GTPase Rac plays multiple roles in epithelial sheet fusion—Dynamic studies of Drosophila dorsal closure *Dev. Biol.* **282** 163–73
- [54] Ladoux B, Mège R-M and Trepat X 2016 Front–rear polarization by mechanical cues: from single cells to tissues *Trends Cell Biol.* **26** 420–33
- [55] Kaunas R, Nguyen P, Usami S and Chien S 2005 Cooperative effects of Rho and mechanical stretch on stress fiber organization *Proc. Natl Acad. Sci USA* **102** 15895–900
- [56] Reffay M, Parrini M-C, Cochet-Escartin O, Ladoux B, Buguin A, Coscoy S, Amblard F, Camonis J and Silberzan P 2014 Interplay of RhoA and mechanical forces in collective cell migration driven by leader cells *Nat. Cell Biol.* **16** 217–23
- [57] Vega F M, Thomas M, Reymond N and Ridley A J 2015 The Rho GTPase RhoB regulates cadherin expression and epithelial cell–cell interaction *Cell Commun. Signal.* **13** 6
- [58] McCormack J, Welsh N J and Braga V M 2013 Cycling around cell–cell adhesion with Rho GTPase regulators *J. Cell Sci.* **126** 379–91
- [59] Zihni C and Terry S J 2015 RhoGTPase signalling at epithelial tight junctions: bridging the GAP between polarity and cancer *Int. J. Biochem. Cell Biol.* **64** 120–5
- [60] Clewley R, Sherwood W, LaMar M and Guckenheimer J 2007 PyDSTool, a software environment for dynamical systems modeling [cited January 18, 2018]. Available from: <https://sourceforge.net/projects/pydstool/>
- [61] Kuramoto Y 1984 *Chemical Oscillations, Waves and Turbulence* (Berlin: Springer) (<https://doi.org/10.1007/978-3-642-69689-3>)
- [62] Strogatz S H 2000 From Kuramoto to Crawford: exploring the onset of synchronization in populations of coupled oscillators *Physica D* **143** 1–20